Drosophila Hamlet mediates epithelial tissue assembly of the reproductive system

Huazhen Wang[1], Ludivine Bertonnier-Brouty[2,3], Isabella Artner[2,3], Jiayu Wen[4,*] and Qi Dai[1,*]

1 Department of Molecular Bioscience, the Wenner-Gren Institute, Stockholm University, Sweden

2 Lund Stem Cell Center, Lund University, Lund, Sweden

3 Lund University Diabetes Center, Lund University, Malmö, Sweden

4 Division of Genome Sciences and Cancer, The John Curtin School of Medical Research, The Australian National University, and Australian Research Council Centre of Excellence for the Mathematical Analysis of Cellular Systems.

[*] Co-corresponding authors

Abstract

Epithelial tissue fusion requires coordinated molecular events at the ends of two epithelial structures. Regulatory mechanisms controlling these events remain largely elusive. In the *Drosophila* reproductive system (RS), this fusion unites the gonad and the genital disc-derived tissues, into a continuous tube. This study unveils the pivotal role of Hamlet (Ham), a *Drosophila* PR-domain containing transcription factor, in orchestrating epithelial tissue fusion in the RS. Loss of *ham* leads to sterility and disconnection between the testes (TE) and seminal vesicles (SV). Systematic analysis of Ham-downstream genes reveals cytoskeletal, metabolic regulators and signaling pathway components. Ham activates genes for epithelial differentiation and remodeling, while repressing genes required for tissue growth and patterning. Using multiplexed in situ hybridization, we demonstrate spatial-temporal gene expression dynamics in contacting epithelia. Key Ham downstream effectors include E-Cadherin (E-Cad), Toll (Tl) and Wnt2 signaling pathways, regulating tissue interaction and fusion. Our findings present a comprehensive gene network crucial for heterotypic epithelial tissue fusion. Mammalian Ham orthologs PRDM3 and PRDM16 are highly expressed in epithelial tissues, suggesting a conserved role across species.

Introduction

Epithelial tissue fusion is a crucial process for building epithelial tubular network and uniting separate ends [1, 2]. Studies from different model systems, like neural tube fusion and *Drosophila* tracheal development, have provided several mechanistic insights into epithelial fusion process. For instance, specialized cells at the leading edge migrate and interact using cytoskeleton protrusions [3-9] and small GTPases like Rac and Cdc42 [10]. Upon contact, the leading cells re-establish polarity and connections with the help of extracellular matrix molecules, apical proteins and E-Cad [11]. However, the exact regulators and mechanisms controlling epithelial fusion remain to be determined, especially in a context-specific manner.

The reproductive system in animals comprises tissues from different origins, and must unite to form a connected system for producing and delivering gametes. For example, the human testis is directly linked to a complex tubular system consisting of the efferent and epididymal ducts [12]. Anomalies in the fusion of these ducts are a significant cause of cryptorchidism, affecting at least three percent of newborn boys. However, there is little understanding of the molecular mechanisms guiding the patterning and fusion of these ducts.

Similarly, the *Drosophila* male RS includes the gonad-derived testis and the genital disc (GD)-formed seminal vesicle, accessory gland (AG), ejaculatory duct (EjD) and additional supportive structures. During development, the TE and SV grow toward each other and merge into a continues tubular system [13]. This involves two epithelial ends, the terminal epithelial cells in the testis and the SV epithelium. While terminal epithelial cells in the testis are specified already in the embryo as male-specific somatic gonadal precursors (msSGPs) [14]. The SV epithelium, together with AG, develops from a group of mesenchymal cells in the GD which undergo mesenchymal-to-epithelial transition (MET) during the larval stage (**Fig. 1A**) [15, 16]. In the developing RS, multiple events, including epithelial tube formation and fusion as well as myoblast and pigment cell migration, are tightly coordinated (**Fig. 1B**) [17]. Thus, the developing *Drosophila* RS provides a representative *in vivo* context to dissect mechanisms underlying epithelial tissue assembly.

Ham belongs to the PR domain containing protein family whose members are evolutionarily conserved cell fate regulators [18, 19]. Dysfunction of the human orthologs of Ham, PRDM16 (Mel1) and PRDM3 (Evi1, MECOM), has been found in a variety of human abnormalities

including congenital diseases, metabolic disorders and cancers [20-27]. Moreover, in at least two types of epithelial cancers (kidney and pancreas cancers), PRDM16 was shown to play a tumor suppressive role [24, 27], indicating its importance in maintaining epithelial integrity. However, it remains undermined how these PR factors regulate epithelial tissue development and homeostasis.

Ham was exclusively studied in the nervous system where it is required for neuronal dendrite morphogenesis [28] and cell fate maintenance [29-31]. Ham was shown to repress gene expression through modulating chromatin states [32] or interacting with the co-repressor CtBP [29, 32]. However, the molecular functions of PRDM16 and PRDM3 are versatile, with their PR domains possessing intrinsic histone methyltransferase activity [21, 33] and the ability to interact with various co-activators and co-repressors [18, 34]. It remains unknown whether Ham plays a role outside of the nervous system and whether Ham also has dual function in gene expression.

In this study, we discovered that Ham is a master regulator in guiding epithelial tissue patterning and fusion in the *Drosophila* RS. Even a slight reduction of Ham disrupts epithelial differentiation and tissue assembly in the RS, ultimately affecting sperm and egg delivery. To explore new mechanisms governing epithelial tissue fusion in the RS, we conducted systematic analyses using RNA-sequencing (RNA-seq), Cleavage Under Targets and Tagmentation (CUT&TAG), multiplexed in situ hybridization data and genetic screening. These analyses led to identification of gene regulatory networks required for epithelial tissue fusion. Ham activates a gene network to promote epithelial cell differentiation and remodeling while suppressing another gene network involved in cell specification and early patterning. These target genes exhibit spatial-temporal expression dynamics during the fusion of the TE and SV. As a key Ham downstream effector, Wnt2 signaling regulates epithelial cell communication and interaction. By elucidating the regulatory network controlled by Ham, our study provides novel insights into the molecular mechanisms underlying epithelial tissue fusion.

Results

132

133 ***Drosophila* RS development is vulnerable to reduced Ham activity**

134

135 While PRDM16 and MECOM are critical cell fate regulators in various developmental
136 contexts in mammals, the genetic roles of Ham were mainly found in the central and periphery
137 nervous systems [28-31]. To systematically study Ham function, we generated new frameshift
138 alleles using CRISPR/Cas9. The sgRNA targets the third exon shared by the three long
139 isoforms B, D and G (**Supplementary Fig. 1A**), producing new alleles specifically disrupting
140 the three PR-domain containing isoforms. We therefore named them $ham^{PR\Delta}$. The original ham^{1}
141 and the null allele ham^{SK1} shifted open reading frame (ORF) for all predicted isoforms [28, 30].

142

143 We validated nucleotide deletions in the new alleles by sanger sequencing (**Supplementary**
144 **Fig. 1B**) and protein deletion by western-blot using an antibody against Ham. The Ham
145 antibody detected several bands in the blot (**Supplementary Fig. 1C**). The two bands at and
146 above the 150KD marker position in the two heterozygotic controls were not detectable in the
147 ham^{SK1} homozygous mutant, suggesting that these two bands correspond to the longest and the
148 second longest isoforms respectively. The $ham^{PR\Delta}$ homozygous samples lack the largest band,
149 verifying the depletion of the longest isoforms. We used one of them (-5nt) for all the later
150 experiments.

151

152 We compared viability and sensory organ development of these alleles. In contrast to the
153 original report showing that *ham* mutant animals died at the larval stage [28], we found that
154 ham^{SK1}, $ham^{PR\Delta}$ and ham^{1} alleles all survived to hatch when combined in trans with the *ham*
155 deficiency line (Df) which deletes the entire *ham* locus (**Supplementary Fig. 1D**). While
156 ham^{1}/Df and ham^{SK1}/Df animals all died right after hatching, about two thirds of the $ham^{PR\Delta}$/Df
157 mutants were viable without obvious gross defects. Furthermore, Ham is known to specify
158 internal cell types (the neuron and sheath) in the sensory organ lineage, as ham^{1} mutants
159 exhibited ectopic external cell types (the socket and shaft) with the expense of internal cells
160 [29]. $ham^{PR\Delta}$ mutants displayed normal sensory organs, in contrast to defective sensory organs
161 in the ham^{1} and ham^{SK1} alleles (**Supplementary Fig. 1E**). Thus, the PR-containing isoforms of
162 Ham are dispensable for sensory organ development and viability.

163

164 However, *ham*$^{PR\Delta}$ mutant animals showed impaired fertility and abnormal morphology in both
165 male and female RS (**Fig. 1D-E, Supplementary 2A-B**). The TE, AG and SV structures were
166 disrupted in males, while mature eggs were stuck in the mutant female ovaries, indicating failed
167 egg delivery. To confirm that the defects are induced by the *ham* mutation, we performed a
168 rescue experiment by utilizing a pBAC transgene that carries the genomic region of *ham* with
169 the super-folding GFP (sfGFP*)* coding sequence in frame with the *ham* ORF. The pBAC
170 transgene rescued the viability of all *ham* mutant conditions, and at least partly restored male
171 fertility of these mutants. Together, these results indicate that the *ham*$^{PR\Delta}$ allele represents a
172 hypomorphic condition which preserves Ham shorter isoforms and partial activity. Thus,
173 although viability and sensory organ development do not require the PR-containing isoforms,
174 formation of the RS depends on them.
175
176 **Ham-expressing epithelial cells connect the gonadal and supportive tissues**
177
178 To examine whether Ham directly controls RS development, we examined Ham expression in
179 the developing RS using a V5 antibody which detects all Ham isoforms in the *ham_V5* allele
180 [35]. Ham_V5 was detected in the connecting tube of the adult SV and TE (**Fig. 1F**).
181 Correspondingly, at the late L3 stage Ham_V5 was detected in the terminal epithelial cells of
182 the TE as well as the btl-Gal4-expressing mesenchymal cells in the genital disc which will give
183 rise to the SV and AG (**Fig. 1G-H**). At the pupal stage, a high level of Ham persists in the TE
184 terminal epithelial cells, SV and AG. In contrast, Ham is barely detectable in the SV myoblasts
185 labeled by the reporter, mef2-Gal4-driving UAS-GFP (**Fig. 1I-J**). Similarly, in the female, high
186 levels of Ham_V5 were found at the joint sites of oviducts and ovaries during both pupal and
187 adult stages (**Supplementary Fig 2C**). Thus, Ham is an intrinsic factor in epithelial cells at the
188 connection site between the gonadal- and genital-disc derived tissues in both males and
189 females.
190
191 **Ham is required for epithelial tissue fusion in the developing male RS**
192
193 The specific expression of Ham and mutant phenotypes in the RS prompted us to investigate
194 its function in RS epithelial tissues. Here we focused on the male, as the assembly of the TE
195 and SV represents a remarkable process involving a series of tissue reorganization events (**Fig.
196 1A-C**). When the two ends of TE and SV get close, the epithelial cells at the leading edges

197 meet and form a common epithelial tube. In the meanwhile, myoblasts from the SV and
198 pigment cells from the TE migrate toward opposite directions, eventually forming distinct cell
199 layers covering both structures.
200
201 We found that at 40-50h APF the TE and SV tubes in *ham^{PRA}/Df and hamSK1/Df* mutants did
202 not properly elongate and appeared shorter and wider compared to that in the wild-type (**Fig.**
203 **2A**). The SV and AG were even unseparated in the *ham* null allele *hamSK1/Df*, suggesting that
204 the severity of RS abnormality correlates with the levels of reduction in *ham* gene products.
205
206 To examine epithelial integrity, we performed immunofluorescent staining using the antibodies
207 against the epithelial cell markers, E-Cad (adherent junctions) and Coracle (Cor, septate
208 junctions equivalent to mammalian tight junction) protein. We also incorporated an SV-
209 specific transgenic reporter, btlGal4-driving UAS-EGFP or UAS-CD8GFP, to the control and
210 *ham* mutant genotypes. E-Cad is enriched at the apical side (the lumen side, **Fig. 2B**) of the TE
211 and SV epithelial tubes. Notably, the TE terminal epithelium accumulates a higher level of E-
212 Cad compared to the SV epithelium, while Cor is mainly expressed at the SV side but not much
213 in the TE, suggesting a heterotypic nature of the TE terminal and SV epithelia.
214
215 Control animals always showed connected TE and SV, whereas *ham* mutant TE and SV tissues
216 were often separated from each other. And even in some mutants where TE and SV tubes were
217 in close contact, they were disconnected (**Fig. 2B**). Importantly, this phenotype can be fully
218 rescued by the *pBAC_ham_sfGFP* transgene, confirming that it is caused by the *ham* mutation.
219 These observations suggest that the epithelial ends of the TE and SV possess distinct properties
220 despite both being epithelial cell types and that Ham is required for TE and SV fusion.
221
222 **Depletion of Ham abolishes TE terminal epithelial cell formation**
223
224 A close inspection on the pupal TE revealed that most of TE epithelial cells were missing in
225 *ham* mutant animals (**Fig. 2B**). TE terminal epithelial cells derive from male specific gonadal
226 precursors (msSGPs) specified in the early embryo (**Supplementary Fig. 3B**) [15] and expand
227 during larval and early pupal stages. *ham* mutant lava either lacked TE epithelial cells or
228 showed abnormal location of these cells, which can be rescued by the *pBAC_ham_sfGFP*
229 transgene (**Supplementary Fig. 3A**). This result indicates that Ham regulates specification or

230 survival of these cells. Indeed, we detected Ham expression in msSGPs and other SGPs in the
231 embryonic gonad. The number of msSGPs labeled by Abd-B or Sox100B-GFP was
232 dramatically reduced in S13 *ham* mutant embryo (**Supplementary Fig. 3C-G**). Thus, Ham is
233 a master regulator for the specification and/ or survival of msSGPs, and the absence of msSGPs
234 accounts for loss of TE terminal epithelial cells in larval and pupal stages.
235
236 **Ham regulates patterning and cell differentiation of the RS epithelial tubes**
237
238 The epithelial cells in the SV and AG originate from a group of mesenchymal cells recruited
239 by the FGF pathway involving Btl and Branchless (Bnl) (**Fig. 1A** and **1H**) [15, 16]. These cells
240 undergo MET to form an epithelial mass which then cavitates to generate inner hollow space
241 and eventually elongates into an epithelial tube. In comparison with the control, the signal
242 intensity of both E-Cad and Crumbs (Crb) were significantly reduced in *ham* mutant SV
243 epithelial cells, which coincides with the shortening of septate junctions labeled by Cor (**Fig.
244 2C-E**). This result suggests that Ham regulates epithelial cell differentiation in the SV. To
245 check whether Ham regulates epithelial cell differentiation in the TE, we used the FRT/FLP
246 system (see Methods) to generate mosaic somatic mutant clones. In these animals, *ham* mutant
247 cells were GFP negative, while wild-type and *ham* heterozygous cells expressed GFP (**Fig.
248 2F**). The E-Cad levels at the border between two mutant cells were significantly lower than
249 those between wild-type cells, indicating that *ham* depletion impaired differentiation of TE
250 terminal epithelial cells.
251 In summary, these phenotypic analyses suggest that Ham controls formation of TE
252 terminal epithelial cells in the early embryo and regulates epithelial tube elongation and cell
253 differentiation at the pupal stage. Thus, failed epithelium fusion in *ham* mutant RS could result
254 from: 1) absence of TE terminal epithelial cells, 2) defects in epithelial tube elongation and cell
255 differentiation of the SV and 3) a combination of both.
256
257 **Ham directly controls epithelial fusion between the TE and SV**
258
259 Next, we sought to assess whether and how Ham directly regulates the fusion process. We first
260 attempted to generate a mild mutant condition which can bypass defects of TE epithelial cell
261 loss and SV-AG tube elongation. We chose RNAi knockdown because knockdown efficiency
262 can be enhanced by overexpressing Dicer2 (Dcr2) and modulated by temperature when RNAi
263 is controlled by the GAL4/UAS system.

We first identified a Gal4 driver expressed in the SV and AG epithelial cells, after screening the available Gal4 transgenes driven by a series of genomic fragments spanning the *ham* locus [36] (**Supplementary Fig. 4A**). This transgene (thereafter named as *hamRSGAL4*) induces high expression of *UAS-GFP* in the TE and SV epithelial cells and neglectable expression in the myoblasts (**Supplementary Fig. 4B**). *hamRSGAL4,* when driving a *ham* RNAi line, nearly abolished Ham expression in animals carrying the *UAS-dcr2* transgene (**Fig. 2G-H,** the middle panels). These animals also had a reduced number of TE epithelial cells and displayed a ball-like structure of the GD, similar to the *ham* null allele. Without *UAS-dcr2*, *ham* RNAi knockdown reduced Ham expression but preserved TE epithelial cells and normal-appearing SV. Remarkably, the TE and SV epithelia still failed to fuse (**Fig. 2H,** the right panel), suggesting that Ham also controls the late step of fusion. Furthermore, E-Cad staining intensity was significantly reduced in *ham* RNAi TE but not in *ham* RNAi SV (**Fig. 2I-J**), suggesting that expression of E-Cad in the TE is sensitive to even mild reduction of Ham protein levels.

Ham controls distinct molecular pathways to promote tissue assembly.

To identify mechanisms that control epithelial fusion, we started to investigate Ham downstream target gene network. We performed RNA-seq experiments from dissected TE and SV tissues during the stage of 18-25h APF. We used two pairs of genotypes, including the wild-type (*wt*), and $ham^{PR\Delta}$ homozygous and the *wt/Df* and *hamSK1/Df* trans-heterozygous (**Fig. 3A**). The comparison between the first pair will determine dysregulated genes in the $ham^{PR\Delta}$ hypomorphic condition, while the comparison between the second pair will identify genes that change expression between the null and *ham* heterozygous conditions.

To not exclude small gene expression changes (*e.g.* in the leading cells which are the minority within the whole tissue), we used a loose cutoff (FDR < 10% and FC>1). We found more than two thousand up-regulated and down-regulated genes in the GD. In the mutant TE, there were similar numbers of dysregulated genes (**Fig. 3B**). The genes that only changed expression in one condition could result from unspecific genetic background, differential dependence on the PR-containing isoforms or different sensitivity to *ham* heterozygous condition.

296 Expression of many dysregulated genes can be indirectly affected by Ham. We next intended
297 to identify genes that are transcriptionally regulated by Ham. To this end, we determined Ham
298 genomic binding sites using Cleavage Under Targets and Tagmentation assays (CUT&TAG)
299 [37] on finely-dissected TE and grossly-dissected abdominal tissues in which Ham is mainly
300 expressed in the TE and SV epithelium (**Fig. 3A**). We used a Ham antibody for wildtype
301 tissues, a GFP antibody for tissues from the *pBAC_ham_SFGFP* transgene and IgG as a
302 negative control in parallel for all the samples. Using the SEACR software, we identified peaks
303 and intersections of peaks across the Ham and GFP antibody conditions (see Methods). For
304 subsequent analyses, only the common 3433 and 691 peaks identified by the two antibodies
305 (Ham and GFP) were included to ensure signal specificity (**Fig. 3C-D**).
306
307 To determine Ham target genes, we intersected the RNA-seq data from the hamSK1/Df versus
308 wt/Df comparison with the Cut&Tag data. Among the 2,546 up-regulated genes in the GD, 441
309 (17.3%) contained Ham CUT&TAG peaks. Among the 2379 downregulated genes, 569
310 (23.9%) showed Ham binding (**Fig. 3E**). In the TE, a lower fraction of dysregulated genes
311 contains Ham CUT&TAG peaks, including 4.7% (108/2274) upregulated genes and 7%
312 (144/2057) downregulated genes (**Fig. 3F**), suggesting that dysregulated genes in the mutant
313 TE are mainly indirectly controlled by Ham.
314
315 Both up- and down-regulated genes contain Ham binding peaks, suggesting that Ham can
316 repress and activate gene expression. To systematically explore the function of Ham-regulated
317 genes, we performed gene network analysis using STRING [38]. We focused on the genes
318 bound by Ham and also dysregulated in the genital disc (GD) in the null condition *hamSK1*,
319 considering that most of TE genes are only indirectly influenced in the ham^{SK1} mutant. The
320 SRING MSL clustering analysis generated 114 functional clusters from down-regulated genes
321 and 62 clusters from up-regulated genes (**Fig. 4A, Supplementary Table 1**). Interestingly,
322 many of downregulated genes clustered into several large groups including cytoskeleton
323 regulators, metabolic factors, cell adhesion and extracellular matrix proteins, suggesting that
324 Ham activates genes to promote epithelial differentiation and remodeling. In contrast,
325 upregulated genes are enriched for patterning factors, cell cycle genes and transcriptional and
326 translational regulators, suggesting that Ham suppresses early developmental processes.
327 Notably, metabolic factors are enriched in both categories, but these factors belong to distinct
328 functional groups. Thus, epithelial fusion requires complex and balanced metabolic processes.

329 Together, this network analysis confirms that Ham positions on top of distinct molecular
330 pathways to facilitate TE and SV assembly.
331
332 Ham was known for its repressive activity via interacting with the co-repressor CtBP and
333 influencing histone modifications [32]. Our finding of its activation function was unexpected.
334 To validate the activation activity of Ham, we chose three downregulated target genes (**Fig.**
335 **4B**), *dwnt2*, *shot* and *shg*, for transcriptional reporter assays. *shg* encodes E-cad, while Shot is
336 a member of the spectraplakin family of large cytoskeletal linker molecules simultaneously
337 binding to actin and microtubules. The function of *wnt2* was reported in the developing RS
338 development [39, 40]. We cloned four genomic fragments from the *wnt2* locus, two each from
339 *shg* and *shot* into a luciferase construct, and co-transfected each reporter with individual
340 plasmids expressing several variants of Ham. In addition to the Ham long isoform and a PR
341 truncation version of Ham, we included the NZF and the CZF domains fused with the VP16
342 activation domain (NZF_VP16 and CZF_VP16) (**Fig. 4C**). The two ZF domains of Ham are
343 putative DNA binding domains, but it remained undetermined whether they help to recruit Ham
344 to DNA. This experimental setting allows to assess which of the ZF domains is able to target
345 Ham-regulated enhancers. The full-length, the PR truncation and the NZF_VP16 fusion all
346 activated expression of the reporters driven by 7 out of 8 Ham-bound elements (**Fig. 4D-G,**
347 **Supplementary Fig. 5A-B**). By contrast, the CZF_VP16 had little activity on the reporters.
348 This result confirms that Ham can directly activate target gene expression and that the NZF
349 domain directly or indirectly recruits Ham to enhancers.
350
351 To further identify co-factors with which Ham interacts to regulate gene expression, we
352 performed *de novo* motif discovery from Ham CUT&TAG peaks in mixed TE and GD tissues
353 close to up-regulated and down-regulated genes in the *hamSK1* mutant using the MEME-ChIP
354 software. This resulted in nine and five significantly enriched motifs from up- and down-
355 regulated gene loci respectively (**Supplementary Fig. 5D**). While five motifs were shared
356 between these two sets, the motifs for Dpp/BMP signaling factor MAD, the zinc-finger protein
357 ZNF263 and two unknown factors were only enriched in the upregulated genes. The result
358 implies that Ham may switch activation to repression activity when interacting with these co-
359 factors in the context of RS development.
360
361 **Ham downstream effector genes are required for male RS fertility.**
362

363 Built upon our transcriptomic data, we next intended to identify genes crucial for the fusion
364 process. We reasoned that as the majority of TE terminal epithelial cells are lost in both *ham*
365 mutant alleles, the commonly downregulated genes in $ham^{PR\Delta}$ and ham^{SK1} TE (**Fig. 3B**) may
366 be expressed in the *wt* TE epithelial cells and can be and functionally important. We thus
367 focused on the top 241 common downregulated genes whose expression showed a fold change
368 greater than 1.5, and the three validated Ham target genes: *shot*, *wnt2* and *shg*. Using all
369 available RNAi lines from the Bloomington stock center that cover 113 out of 244 candidate
370 genes, we performed a UAS-RNAi screen with the *UAS-dcr2*; *hamRSGal4* driver for male
371 fertility (see Methods).
372
373 The RNAi screen led to identification of 26 genes whose knockdown abolished or reduced
374 male fertility (**Supplementary Table 2**). Knocking down four of these genes, *shg*, *AP2-alpha*,
375 *pebble (pbl)* and *CG11406*, resulted in complete sterility, indicating their importance for male
376 fertility. We defined this category as 100% penetrance of sterility. Knockdown of other twenty-
377 two genes reduced fertility to different extent (**Fig. 5A-B**).
378
379 Consistent with the gene network analysis (**Fig. 4A**), these genes include cytoskeleton
380 regulators (*pbl*, *shg*, *shark*) [41-43] and metabolism factors (*CG11406, Ph4alphaMP, GstE11,*
381 *CG17477, CG11069, AdSL, CG17283, CG15117, CG7484*). Other genes are known or
382 predicted to be involved in intracellular membrane trafficking (*AP-2alpha*, *CG31935* and
383 *CG7456*) [44] and signaling (*wnt2*, *Toll*, *AkhR*, *Idgf4* and *Hr46*) [45-48].
384
385 We confirmed that knocking down *pbl*, *AP-2alpha, CG11406* and *shg* led to failed TE and SV
386 fusion and abnormal morphology at the pupal stage (**Fig. 5C)**. *pbl* encodes a Rho guanine
387 nucleotide exchange factor, implicated in multiple processes involving cytoskeleton
388 reorganization[41, 49, 50]. The gene product of CG11406 is a predicted triglyceride lipase,
389 cleaving triacylglycerol (TAG) to produce diacylglycerol (DAG). AP-2alpha, a subunit in the
390 Adaptor complex 2, is involved in intracellular trafficking and secretion [51]. Remarkably, *shg*
391 knockdown also led to aberrant mobilization of TE epithelial cells to the middle of the TE,
392 while no such effect was found in the SV and AG. Downregulation of E-Cad is a key event
393 during epithelial to mesenchymal transition (EMT), and E-Cad promotes cohesive cell
394 migration of mesenchymal cells, but suppressing cell motility of epithelial cells [52, 53]. Our
395 result suggests that the SV and the TE terminal epithelia have distinct dependence on E-Cad

396 and that TE epithelial cells are prone to becoming motile when E-Cad is reduced. Together,
397 this screen identified a collection of known and novel factors involved in epithelial tissue
398 fusion, confirming that the fusion process requires coordinated activity of several classes of
399 molecules.
400
401 **Ham downstream genes exhibit spatial- temporal expression dynamics in the male RS**
402
403 During epithelial fusion, cells at the leading edge become specialized and express specific
404 genes required for tissue interaction and remodeling [1, 2]. Moreover, as we observed, the TE
405 terminal and SV epithelia have distinct properties, suggesting that these two sets of epithelial
406 cells may express distinct genes. We thus intended to assess spatial distribution of Ham
407 downstream genes. We conducted a high-resolution multiplexed RNA *in situ* hybridization
408 assay known as SCRINSHOT (single cell RNA *in situ* hybridization on tissues) [54] to
409 visualize expression of candidate genes including *wnt2*, *shg*, *shot* and other positive genes from
410 the RNAi screen, along with the receptor genes in Wnt2 signaling (*fz*, *fz2*, *fz3* and *fz4*) and
411 ligand genes in Tl-signaling (*spz*, *spz4*, *spz5* and *spz6*) (**Supplementary Table 3**). Some of
412 these Wnt2 and Tl signaling genes displayed dysregulation in at least one of the *ham* mutant
413 alleles according RNA-seq data (**Supplementary Fig 6A-B**). Other receptor genes in Wnt
414 signaling and ligand genes in Tl signaling were omitted due to low read numbers in the RNA-
415 seq data, indicating negligible or minimal expression in the TE and GD.
416
417 Each SCRINSHOT reaction took place within a mini-chamber, accommodating pairs of control
418 and *ham* mutant tissues, or GFP KD control and ham RNAi KD samples (refer to Methods for
419 details of probe design and experimental procedures). This setup was designed to minimize
420 technical variability between the genotypes. mRNAs are visualized as fluorescent dots in
421 SCRINSHOT images, with each dot representing a single mRNA molecule. However, due to
422 the densely packed nature of cells in the TE and SV tissues, quantifying mRNA molecules at
423 a single-cell resolution is challenging. Therefore, we opted to quantify fluorescent signal
424 intensity within defined areas (see Methods). In total, 37 genes were tested, including *ham*
425 itself (**Supplementary Table 3**). Probes for 7 genes gave either no or low signal in the TE or
426 GD, likely attributed to poor probe quality, given their RNA-seq read numbers not being low.
427 Resembling Ham protein expression (**Fig. 1G**), *ham* mRNAs were detected in the TE terminal
428 epithelium (**Fig. 6A**), confirming the specificity of the SCRINSHOT method. Similarly, *wnt2*,
429 *shg* and *shot* all exhibited high expression in the TE terminal epithelium (**Fig. 6A**).

430

431 In total, 25 genes exhibited detectable SCRINSHOT signal in the wt SV and AG, while 29
432 displayed signals in the wt TE (**Supplementary Table 3)**. Within the TE, 17 out of 29 were
433 specifically localized in the TE terminal epithelial cells, with the remaining 12 detected only
434 in other TE cells (**Fig. 6, Supplementary Fig. 7, Supplementary Table 3**).

435

436 Subsequently, our analysis focused on the genes expressed in the TE terminal and SV epithelia.
437 While 17 genes exhibited expression in both epithelial ends (**Fig. 6A-B**), 8 were exclusively
438 expressed in SV epithelial cells (**Fig. 6F**, **Supplementary Table 3**), underscoring the
439 heterotypic nature of the TE and SV epitheliums. Notably, certain genes (CG11406, *AP-*
440 *2alpha*, *GstE11*, *Tl, spz5* and *spz6*) demonstrated temporal dynamic expression in the TE
441 epithelium: spz5 and CG11406 are present during the 20-25h APF timeframe, prior to fusion,
442 but gone during the 28-32h APF period when the TE and SV are undergoing fusion; *AP-2alpha*,
443 *GstE11*, *Tl* and *spz6* showed the opposite trend, being expressed only later (**Supplementary**
444 **Fig. 7B**).

445

446 In the GD, while the majority of genes exhibited ubiquitous expression, *wnt2* and *spz* were
447 predominantly expressed in the leading cells within the SV, contrasting with their expression
448 in the remaining GD (**Fig. 6B**). Additionally, the expression patterns of *fz2*,*fz3* and *Tl* displayed
449 spatial specificity: fz2 exhibited higher expression levels in the SV compared to the AG, *fz3*
450 demonstrated the opposite pattern with higher expression in the AG, and *Tl* was primarily
451 expressed in the myoblasts (**Fig. 6B**). These findings imply that Wnt2 and Tl signaling may
452 have cell-type-specific roles in the fusion process. Thus, SCRINSHOT mapped 30 candidate
453 genes in the developing GD and TE, with 29 of them display spatial or temporal dynamics.

454

455 **Wnt2 and Tl signaling pathways are key mediators of Ham function in RS tissue assembly**

456

457 Next, we aimed to identify genes exhibiting altered expression in *ham* mutant SV and TE. As
458 *hamSK1* mutant TE lacks terminal epithelial cells, we excluded TE samples and only quantified
459 SCRINSHOT signal levels in the developing SV between *wt* and the *hamSK1* mutant. In
460 contrast, *ham* RNAi knockdown resulted in fusion defects but only mildly impacted SV
461 morphology and TE terminal epithelial cell number (**Fig. 2G-H**). These samples allow to assess
462 gene expression alterations in both the SV and TE epithelia.

463

464 *ham* fluorescent intensity appeared comparable between *wt* and mutant samples (**Fig. 6E,**
465 **Supplementary Fig. 7E**), suggesting that *ham* mutant RNAs, containing the CRISPR-
466 generated indels, remain stable at this stage. In the *hamSK1* mutant SV, seven genes became
467 downregulated, while two exhibited upregulation. The downregulated genes were four Wnt2
468 pathway genes (*wnt2, fz, fz2, fz4*), one Tl pathway gene (*spz*), and *shg* (**Fig. 6B-**C). Notably,
469 *wnt2*, *fz*, *spz* and *shg* also displayed downregulation in *ham* RNAi SV (**Fig. 6D-E**), suggesting
470 that these genes and their associated signaling pathways may be directly involved in the fusion
471 process downstream of Ham. The upregulated genes in *hamSK1* mutant SV include *GstE11*
472 and *CG11069* (**Supplementary Fig.7C, E**), which exhibited low expression in the leading cells
473 of wt SV epithelium, but increased expression under the *hamSK1* condition. In *ham* RNAi
474 knockdown animals, *CG11069* was again upregulated, while *GstE11* did not change
475 expression. Instead, another ligand gene in Tl signaling (*spz5*) displayed increased expression
476 (**Supplementary Fig.7D, F**). On the TE side, only four genes showed expression alteration in
477 *ham* RNAi animals, including *ham* itself, *shg*, *fz* and *fz2* **Supplementary Fig.7G**), implicating
478 functional requirement of these genes in both TE and SV epithelia.
479
480 The observation that knocking down Tl resulted in decreased male fertility (**Fig. 5B**,
481 **Supplementary Table 2**), coupled with the expression of multiple *spz* ligand genes in the
482 developing TE and SV, suggests that the Tl signaling pathway might be required for assembling
483 the TE and SV. To investigate this possibility, we examined male flies with *spz* knockdown
484 driven by *hamRSGal4*. These animals produced a comparable number of progenies to control
485 animals. The lack of phenotype in this condition could be attributed to inefficient knockdown
486 or genetic compensation by another *spz* gene, like *spz5* whose expression increased in *ham*
487 RNAi animals when *spz* expression was reduced. In addition to Tl, two other Tl related genes
488 (Toll-7 and Toll-9) exhibited moderate number of reads in the RNA-seq data. We then tested
489 male fertility in *Toll-7* and *Toll-9* knockdown animals. *Toll-9* knockdown led to a drastic
490 reduction in progeny numbers compared to the RNAi control (**Supplementary Fig. 8A**).
491 Consistent with the sterility, the adult SV in the *Toll-9* knockdown male lacked sperms
492 (**Supplementary Fig. 8A**), suggesting failed connection between the TE and SV. Together,
493 these results pinpoint an essential role of Tl signaling in male RS development.
494
495 To validate the role of Wnt2 signaling in RS development, we investigated four genetic
496 conditions, aimed at modulating its level and activity: $wnt2^{O}$ (a *wnt2* null allele), *wnt2*
497 overexpression driven by *hamRSGal4*, *fz* and *fz2* RNAi knockdown driven by *hamRSGal4*. The

498 *wnt2^{O}* mutant TE and GD never connect, suggesting that Wnt2 is essential for the fusion
499 process. The *wnt2^{O}* mutant TE lacks the pigment cell and myocyte layers (**Fig. 7A**), consistent
500 with its reported function in these two cell types [17, 39]. The *wnt2^{O}* mutant GD failed to form
501 elongated SV and AG, suggesting that Wnt2 is required for GD patterning and differentiation.
502 Moreover, overexpression of *wnt2* also resulted in fusion defects and mis-localization of TE
503 epithelial cells (**Fig. 7B**), a phenotype reminiscent of *shg* knockdown animals. Indeed, *wnt2*-
504 overexpressing cells displayed reduced levels of E-Cad, suggesting that Wnt2 signaling might
505 balance E-Cad levels to maintain TE epithelial cell properties. Consistently, *fz2* knockdown
506 animals exhibited comparable phenotypes, including mobilized TE epithelial cells and failed
507 tissue fusion (**Fig. 7C**). *fz2* and *fz* knockdown also decreased male fertility (**Fig. 7D**).
508 Collectively, these results suggest the importance of optimal Wnt2 signaling levels in male RS
509 development and epithelial tissue fusion.
510
511
512
513
514
515
516
517
518
519
520
521
522
523
524
525
526
527
528
529
530
531

532 **Discussion**

533

534 In this study we demonstrate that the transcription factor Ham plays a crucial role in controlling
535 epithelial fusion during *Drosophila* RS development. Early in embryonic development, Ham
536 determines the cell fate of msSGPs, which are progenitor cells for TE terminal epithelial cells.
537 Later on, Ham directly regulates the differentiation of epithelial cells in both the TE and SV by
538 orchestrating a gene expression program in epithelial cells. While our primary focus is on male
539 RS, we found that Ham is also expressed in cells at the fusion site of the oviduct and ovary.
540 Mutant females lacking functional Ham exhibit a non-functional oviduct epithelial tube,
541 suggesting that Ham likely employs a similar mechanism to control epithelium fusion in
542 females.

543

544 By examining *ham* mutant phenotypes and its downstream target genes, we identified several
545 classes of novel factors involved in fusion process of SV and TE. These genes, directly or
546 indirectly controlled by Ham, encompass a diverse array of molecular functions. This discovery
547 provides a comprehensive gene network for future investigation of epithelial fusion processes.
548 The cell-type-specific and tissue-specific spatial distribution of these genes suggest that they
549 may regulate various aspects of fusion, including cell migration, intercellular communication
550 between myoblasts and epithelial cells, specification of the leading cells, and other steps in the
551 fusion process. For instance, Tl and its related receptors is known to mediate cell adhesions
552 [55]. We can speculate that Tl signaling and the molecule itself promote interaction between
553 myoblasts and myoblast and epithelial cells (**Fig. 7E**), based on high expression of Tl in
554 myoblasts and presence of multiple Spz ligands in the TE and SV epithelial cells. Moreover,
555 *Wnt2*, *fz* and *fz2* are highly expressed in the leading cells of TE and SV epithelia, and also
556 required for TE and SV connection, suggesting that Wnt2 signaling mediates epithelial cell
557 communication, remodeling and fusion.

558

559 Despite being discovered more than twenty years ago [28], research on the function of Ham
560 function has primarily focused on its roles in the nervous system. Our findings highlight a
561 crucial function of Ham in epithelial tissues. Apart from the RS, we observed high expression
562 of the Ham protein in other epithelial tissues including the Malpighian tubes (akin to the kidney
563 in insects) and the intestine (data not shown). Furthermore, orthologs of Ham, PRDM16 and
564 PRDM3/MECOM, exhibit high expression in epithelial tubular structures, such as Lung,
565 pancreas, kidney, urinary bladder and gastrointestinal tract and lung, according to observations

566 in the Human Protein Atlas (**Supplementary Fig. 9**.
567 https://www.proteinatlas.org/ENSG00000142611-PRDM16/single+cell+type;
568 https://www.proteinatlas.org/ENSG00000085276-MECOM/single+cell+type) [56]. Notably,
569 Seminal vesicle and ductus deferens, the equivalent structure to fly seminal vesicle, are the top
570 one and three tissues with the highest PRDM16 expression (**Supplementary Fig. 9A**). This
571 suggests a potential role for these proteins in controlling epithelial integrity and fusion in
572 mammalian organogenesis. Indeed, we observed that the pancreas duct volume in mouse
573 embryos lacking *Prdm16* is significantly reduced (data not shown). Although the exact cellular
574 changes and the underlying molecular mechanisms in this context await further investigation,
575 this phenotype underscores a crucial function of *Prdm16* in pancreatic epithelial duct
576 formation.
577
578 We show that compared to Ham function in the nervous system, the PR-containing isoforms
579 are indispensable for RS epithelial fusion and differentiation, and that Ham can directly activate
580 epithelial gene expression. It remains to be determined whether Ham has distinct molecular
581 functions or it regulates a subset of common molecular pathways in these two contexts.
582 Dendrite morphogenesis involves outgrowth and branching, somewhat analogous to epithelial
583 tube growth and branching. For instance, molecular mechanisms regulating polarized protein
584 trafficking are crucial for both dendrite and epithelial tube branching [57]. Additionally, several
585 transcription factors like Sequoia [58, 59], Tramtrack [60, 61] and Cut [62, 63] play roles in
586 both dendrite morphogenesis and tracheal tube fusion. These examples suggest that there might
587 be more unrecognized common mechanisms between dendrite and epithelial morphogenesis.
588 It is of interest to test whether the effectors we identified in the RS epithelium are involved in
589 dendrite morphogenesis in the nervous system.
590
591 We observed a unique aspect of epithelial fusion in the *Drosophila* RS. Unlike many epithelial
592 fusion processes where two homologous ends merge, such as those in mammalian neural tube
593 closure and *Drosophila* tracheal formation *etc* [1, 8, 10], the two epithelial ends in the
594 *Drosophila* RS are heterotypic. Specifically, the TE terminal epithelial cells express higher
595 levels of E-Cad and lower levels of Cor compared to SV epithelial cells. In response to the
596 reduction of E-Cad or ectopic expression of *wnt2*, TE terminal epithelial cells become motile,
597 resembling a process akin to epithelial-to-mesenchymal transition. This suggests that TE
598 terminal epithelial cells may be more invasive during epithelial fusion. On the other hand, SV
599 epithelial cells, despite originating from mesenchymal cells, exhibit typical epithelial cell

characteristics, including regular Cor and E-Cad expression. Notably, many genes are expressed exclusively in the SV epithelium, distinguishing it from the TE epithelium. Heterotypic epithelial fusion occurs in many developmental processes, such as digestive system formation, vertebrate optic fissure closure, and mammalian urogenital development. Failure of epithelial fusion can lead to a wide variety of developmental diseases such as oesophageal atresia, spina bifida, ocular coloboma, congenital abnormalities of the kidney, urinary tract and persistent cloaca. Studying the basic processes and key players of normal epithelial tissue fusion in an *in vivo* context will help to understand the pathogenesis of these diseases.

Acknowledgements

We thank the imaging facility (IFSU) of Stockholm University, the BEA sequencing facility at Karolinska Insitute, and the National Genomic Institute of Scilife Laboratories, Sweden, for providing service and support. The Bloomington Stock Center and the *Drosophila* community provided important reagents and fly stocks. We thank Christos Samakovlis's lab for helping to set up SCRINSHOT and Eric Lai's lab for the initial Ham reagents. Funding from Australian Research Council Centre of Excellence for the Mathematical Analysis of Cellular Systems (CE230100001) and ANU Future Scheme to J.W. The project was supported by project grant from Swedish Research Council (Vetenskapsrådet, 2020-03543) and Swedish Cancerfonden (CAN 22 2161 Pj) to Q.D.

Author contributions

Conceptualization and project design by QD, experiments conduction by HW, preliminary test in pancreas by IA and LB, computation analysis by JW. Data interpretation by HW, JW and QD. Manuscript writing by QD with input from HW and JW.

634 **Materials and methods**

635

636 ***Fly strain culturing and generation of transgenes***

637 All fly stocks were maintained at 22°C. The *ham*$^{PR\Delta}$ mutants were created using CRISPR:
638 transgenic flies carrying single guide RNA targeting the PR domain containing isoforms were
639 crossed into the vas-Cas9 transgenic flies. Frame-shift mutations were identified by PCR and
640 Sanger sequencing. Transgenic flies were created at BestGene, Inc.

641

642 The ham Gal4 lines and RNAi stocks were obtained from Bloomington Stock Center.
643 Knocking down experiments were performed at 25 °C and with a regular 12-hr light–dark
644 cycle.

645

646 To generate ham null mutant somatic clones in the TE terminal epithelium, *hamsk1*
647 *FRT40A/CTG* males were crossed with virgin females carrying the genotype *hsFLP(X);*
648 *hsGFP.nls FRT40A.* Embryos aged 0-5 hours were collected and developed at 25°C until the
649 2nd instar larval stage. GFP-negative larvae, indicating the genotype *hsFLP(X);*
650 *hsGFP.nls/hamsk1 FRT40A*, were then selected. Head shock treatments at 37°C for 1 hour
651 were administered three times during the 2nd and 3rd instar larval stages to induce somatic
652 clones. Prior to dissection, another 1-hour head shock at 37°C was performed to induce GFP
653 expression, marking the wild-type cells.

654

655 ***Fertility test***

656 For ham mutants, single male or female with indicated genotype was mated with
657 two w^{1118} virgin females or two w^{1118} males on day 0 of the experiment. Crosses were flipped
658 every 2 days for 3 consecutive times. Progenies from the second vial with eggs laid between
659 day 2-4 were counted after 2 weeks.

660

661 For the RNAi screen, individual UAS-RNAi males were crossed with females carrying UAS-
662 dcr2 and hamRSGal4. The resultant F1 male progenies (2-5 days old) with the genotype UAS-
663 dcr2; hamRSGal4>UAS-RNAi were crossed to w^{1118} virgin females (1-2 days old) on day 0 of
664 the experiment. In each test, four males were crossed with three females. Crosses were flipped
665 on day2 and day3 for pre-laying. After flipping on day3, crosses were kept in the new vial for
666 egg laying for a specific time period (GroupA: 48hours; GroupB: 16-18h; GroupC: 7-8h). If at

667 least three males and two females were alive, then the flies were transferred to a new vial, the
668 old vial was kept, and all progenies were counted.
669
670 For fertility test of the Wnt2 and Tl signaling pathways components, UAS-RNAi males were
671 crossed to virgin females of the genotype UAS-dcr2; hamRSGal4. Two F1 male progenies (1-
672 2 days old) with the genotype UAS-dcr2; hamRSGal4>UAS.RNAi were crossed to three w^{1118}
673 virgin females (1-2 days old) on day 0 of the experiment. Crosses were flipped every day for 4
674 consecutive times. Progenies from the forth vial with eggs laid between day 3-4 were counted
675 after 2 weeks. Crosses were flipped every day for 4 consecutive times. Progenies from the forth
676 vial with eggs laid between day 3-4 were counted after 2 weeks.
677
678 ***Immunostaining***
679 For embryo staining: embryos were collected, dechorionated with bleach and fixed with 4%
680 formaldehyde in PEM (0.1M PIPES, 2mM EGTA, 1 mM MgSO4, pH 7) for 20 min. For
681 immunostaining, embryos were rehydrated, washed with PBT (0.3% Triton X-100 in PBS) and
682 blocked with PBSBT (0.3% Triton X-100, 1% BSA in PBS).
683
684 For tissue staining: tissues were dissected from stage defined larvae or pupae in 1xPBS within
685 30 min and fixed in 4% paraformaldehyde in PBS for 20min. For immunostaining, dissected
686 tissues were washed with PBT (0.1% Triton X-100 in PBS) and blocked with PBSBT (0.1%
687 Triton X-100, 1% BSA in PBS).
688
689 For both embryo and tissue staining, the primary antibodies were diluted with PBSBT (0.1%
690 Triton X-100, 1% BSA in PBS) and incubated at 4°C over night. After extensive washing with
691 PBSBT (15min x 4 times), the secondary antibodies were added in 1:500 dilution and incubated
692 at room temperature for 2h. After washing with PBT (0.1% Triton X-100 in PBS), the samples
693 were counter-stained with DAPI and mounted in Vectashield (Vector Laboratories).
694
695 The following primary antibodies were used: Rabbit anti-Ham (1:300) (Gift from Eric Lai's
696 lab), Ms anti-V5 (1:500, R960-25, invitrogen), chk anti-GFP (1:2000, ab13970, Abcam), Rat
697 anti-vasa (1:50, anti-vasa-c, Developmental Studies Hybridoma Bank, DSHB), Ms anti-ABD-
698 B (1:50, 1A2E9-c), Ms anti-SXL (1:50, M18-c), rat anti-DE-Cad (1:50, DCAD2, DSHB),
699 mouse anti-Crb (1:10, Cq4 DSHB), mouse anti-Coracle (1:100, C615.16 DSHB). Secondary

700 antibodies conjugated to Cy3 or Cy5 or Alexa Fluor-488 (Jackson ImmunoResearch) were
701 used.
702
703 ***Quantification of signal intensity from fluorescent immunostaining***
704
705 For E-Cad and Crb in Figure 2, "raw intensity density" from manually defined regions (using
706 free-hand drawing) along the apical side of the SV and TE terminal epitheliums was obtained
707 in ImageJ. For each sample, 2 regions in the SV and 3 regions in the TE terminal epithelium
708 were averaged. The regions used to determine relative E-Cad fluorescence in *hamSK1* TE
709 somatic clones were at the apical side between cell junction. The length of Cor-stained cell
710 junction was measured using ImageJ. A straight line was drawn over the Cor staining with the
711 'Freehand Line tool'. For each sample, the average length from 10 cell-cell junctions were
712 used. In all experiments, images for the genotypes in comparison were always processed using
713 exact settings. At least three biological replicates were included in statistical analysis.
714
715 ***Western Blot***
716 Embryos from *w1118,* $ham^{PR\Delta}$*/CTG,* ham^{SK1}*/CTG* were collected and aged to embryonic stage
717 S13 to S16. In each blot, 50-100st GFP+ or GFP- embryos were used. The selected embryos
718 were homogenized directly in 1xSDS loading buffer (62.5 mM Tris-HCl pH 6.8, 2.5 % SDS,
719 0.002 % Bromophenol Blue, 0.7135 M (5%) β-mercaptoethanol, 10 % glycerol) and denatured
720 at 98 °C heat blot for 5 min. After centrifuged, supernatant was taken for Western-Blotting
721 with 8% of SDS-PAGE. Rabbit anti-Ham (1:2000) primary antibody was used in blotting. To
722 minimize unspecific signal from IgG heavy chains, light chain specific secondary antibody of
723 mouse anti-Rabbit IgG (1:40000 Jackson ImmunoResearch) was used, and the signals were
724 developed with ECL Plus reagent (GE Healthcare).
725
726 ***Cell culture and Luciferase assays***
727 To generate different variants of Ham, the open reading frames of HamFL, Ham-NZF-vp16,
728 Ham-CZF-vp16, and $ham^{PR\Delta}$ were PCR amplified and cloned into the pAC_V5 (nitrogen)
729 vector. The enhancer fragments were cloned in to the p2xTetO-Firefly luciferase vector. All
730 transfections were performed using *Drosophila* S2-R+ cells grown in Schneider *Drosophila*
731 medium containing 10% fetal calf serum. Cells were co-transfected with the Ham expression
732 construct, 2xTetO-Firefly luciferase and pAc-Renilla plasmids in 96-well plate using the

733 Effectene Transfection kit (Qiagene). Luciferase assays were performed and measured using
734 the Dual Luciferase Assay System (Promega). Expression was calculated as the ratio between
735 the firefly and *Renilla* luciferase activities. Three rounds of transfections were performed on
736 different days and different cell populations and considered as three biological replicates.
737 Within each biological replicate, 4 wells of cells were transfected with the same DNA mixture
738 and measured and thus considered as 4 technique replicates. In total, for each DNA
739 combination, the values from the 12 wells of transfection were calculated, averaged and plotted
740 in Fig. 5D-F. Cloning oligos are provided in **Supplementary table 4**.
741
742 ***SCRINSHOT***
743 The Drosophila reproductive system was dissected at defined ages in 1xPBS and fixed in 4%
744 paraformaldehyde in PBS for 20min. After washing with PBST 0.1% (Triton X-100) for 2 x
745 15 min, fine dissected samples were placed on Poly-lysine coverslip and freezed at -80°C after
746 drying on a heater.
747 The SCRINSHOT experiments were carried out according to the published method [54]. In
748 brief, 3 padlock probes and 3 corresponding detection probes were designed for each gene of
749 interest. The slides with fine dissected samples were pretreated at 45˚°C to reduce moisture and
750 fixed in 4% PFA in 1X PBS, followed by washing in PBS Tween-20 0.05% twice. Samples
751 were then dehydrated with 70%, 85%, 100%ETOH and air dry. The SecureSeal hybridization
752 chamber (GRACE BIO-LABS, 621501) was then mounted to cover samples on the slide.
753 Permeabilization of tissues were first done by treating with 10µg/mL Proteinase K (Invitrogen)
754 in PBSTween-20 0.05% for 7 minutes followed by washing with Glycine (2mg/mL in PBS
755 Tween-20 0.05%) once and with PBS Tween-20 0.05% for 3 x 5 minutes. After this, samples
756 were further Permeabilized in 0.1M HCl for 3min, followed by washing in PBS Tween-20
757 0.05% twice. Samples were then blocked in a probe-free hybridization reaction mixture of
758 1XAmplifase buffer (Lucigen, A1905B), 0.05M KCl, 20% Formamide deionized (Millipore
759 S4117), 0.1uM Oligo-dT, 0.1ug/ul BSA (New England Biolabs, B9000S), 1U/ul RiboLock
760 (Thermo, EO0384), and 0.2ug/ul tRNAs (Ambion, AM7119). Then hybridization of padlock
761 probes was done by incubating samples with padlock probes (with the concentration of each
762 one 0.01uM) mixed in blocking reagents used before (no oligo dT used in this step). The slide
763 was then put into a PCR machine to denature at 55˚C for 15 minutes and hybridize at 45˚C for
764 120 minutes. Padlock probes were then ligated by using SplintR ligase (NEB M0375) at 25˚C
765 for 16 hours followed by RCA (rolling cycle amplification) at 30˚C for 16 hours by using phi29
766 polymerase (Lucigen, 30221–2) and RCA primer1. Then a fixation step was applied to stabilize

767 RCA product in 4% PFA for 15 minutes followed by washing in PBS Tween-20 0.05%. Then
768 the hybridization of the first 3 genes was done by mixing all 3 3' fluorophore-conjugated
769 detection probes of each gene in reaction reagent (2XSSC, 20% Formamide deionized, 0.1ug/ul
770 BSA, and 0.5 ng/µl DAPI (Biolegend, 422801) followed by hybridization at 30˚C for 1 hour.
771 The slides were washed in 20% formamide in 2X SSC and then in 6X SSC, followed by
772 dehydration in 70%, 85%, 100% Ethanol until the chamber was removed. Then the samples
773 were preserved in SlowFade Gold Antifade mountnant (Thermo, S36936) and kept in dark
774 before imaging. After image acquisition, the first 3 detection probes were removed by using
775 Uracil-DNA Glycosylase (Thermo, EN0362), and the slides were ready for the next round of
776 detection probe hybridization. The procedure was repeated until all genes were hybridized and
777 imaged. Images were acquired with an airyscan-equipped confocal microscope system (Zeiss
778 LSM 800, Carl Zeiss), and ZEN 2.5 Blue edition software was used for image processing.
779
780 ***Quantification of SCRINSHOT signals***
781 Similar to quantification of immunofluorescent signal, fluorescence intensity of SCRINSHOT
782 for each gene was measured in defined areas within images of the SV, EjD, and TE in 2D
783 projections. Squares were drawn to define areas at the leading side of the SV, the middle region
784 of the Ejd and the TE terminal. The total fluorescence intensity was first normalized to area
785 size. The resultant value for *ham* mutant or RNAi samples was then contrasted to the
786 normalized intensity of control samples.
787
788 ***CUT&TAG***
789 CUT&TAG was performed according to the published method [37]. In brief, TE and grossly
790 tissue of the posterior abdomen were dissected from 18-25h APF *w1118* and
791 *pBAC_ham_sfGFP* animals in PBS within 30 min. For grossly tissues, the dissected samples
792 were homogenized in 2ml NE1 buffer followed by incubation on ice for 10 min. After filtering
793 out the grossly cuticles, nuclei were collected by spinning at 1300xg and resuspended in 1ml
794 PBS. For TE, nuclei extraction was done by simply pipetted samples in 200ul NE1 up and
795 down for 20-30 times and incubated on ice for 10 min. Light fixation was performed with 0.1%
796 formaldehyde at RT for 2 minutes and neutralized with 75mM Glycine. Then the nuclei were
797 washed by PBS and wash buffer 1 time each and kept in 200ul wash buffer on ice until enough
798 samples were collected (30-50st animals per/antibody). Resuspended nuclei in 1.2ml wash
799 buffer and mixed with 20ul Concanavalin A-coated magnetic beads (Polyscience 86057) with
800 soft vortexing. Aliquoted samples into two parts immediately and incubated for 10 min with

801 rotation to allow the binding of the nuclei with the beads. The nuclei/beads mix was then
802 blocked with 1mL cold antibody buffer for 10 min and resuspended in 150ul cold antibody
803 buffer. For w1118 samples, 1uL Rabbit anti-Ham or 1ul Rabbit IgG (SIGMA-ALDRICH,
804 I5006) was added for an overnight incubation at 4°C. For *pBAC_ham_sfGFP* samples, 1ul
805 Rabbit anti-GFP (G10362, invitrogen) or Rabbit IgG was used. The beads/nuclei/antibody mix
806 was then washed with Dig-wash buffer and incubated with secondary antibody (1:100 dilution)
807 for 1 hour. After further washes with the Dig-wash buffer, a pA-Tn5 adaptor complex in Dig-
808 300 buffer was added to the beads for 1 hour reaction. The beads were then washed with Dig-
809 300 buffer before the incubation with 300ul Tagmentation buffer at 37°C for 1 hour. Then 10ul
810 0.5M EDTA, 3uL 10% SDS and 2.5uL 20 mg/mL proteinase K (Invitrogen) were used to stop
811 the reaction. Then the resultant DNA was purified with DNA clean & Concentrator kit (ZYMO
812 Research D4013) and eluted in 25uL Elution buffer. To generate libraries, 21uL fragment DNA
813 was mixed with 2uL 10uM Universal i5 primer, 2uL 10uM uniquely barcoded i7 primer and
814 25uL PCR master mix (NEB Phusion® High-Fidelity PCR Master Mix with HF Buffer,
815 M0531). The PCR condition was as follows: 72°C 5min, 98°C 30s, repeat 12 times (98°C 10s,
816 63°C 10s), 72°C 1 min and hold 4°C. The libraries were cleaned with standard Ampure XP
817 beads as previously described. Libraries from four biological replicates were produced for each
818 condition.
819
820 We mapped the CUT&TAG samples of *w1118* and *pBAC_ham_sfGFP* in TE and TG tissues
821 to the dm6 genome assembly using Bowtie2 with the following parameters: bowtie2 --end-to-
822 end --very-sensitive --no-mixed --no-discordant --phred33 -I 10 -X 700. The coverage for these
823 samples was generated using bedtools genomeCoverageBed and normalized to library depth to
824 yield reads per million per base (RPM). For peak calling, we employed SEACR [64], which is
825 tailored for sparse chromatin profiling data like CUT&TAG. We first used a relaxed FDR
826 cutoff of < 0.5 for each replicate (SEACR_1.3.sh normalized_coverage 0.5 norm stringent
827 output_peaks), we then identified common peaks across replicates for each condition. To select
828 confident peaks for *w1118* and *pBAC_ham_sfGFP*, we overlapped their peaks within TE and
829 TG separately, choosing the top 1800 peaks from TE and the top 6000 from TG. Peak
830 annotation was performed by HOMER's annotatePeaks.pl. Peak overlap analysis was
831 performed using HOMER's mergePeaks function with the default -d given parameter, ensuring
832 that only directly overlapping peaks were merged. This method preserved the integrity of the
833 original peak boundaries and maintained the specified distances between peaks from the initial
834 peak calls. *De novo* motif discovery for peaks in up-regulated or down-regulated genes,

835 positioned 2000 bp upstream and 500 bp downstream of the TSS in TE and TG tissues, was
836 performed using the MEME-ChIP software. The parameters used were: -ccut 100, -meme-p 5,
837 -dna, -meme-mod anr, -minw 5, -maxw 15, and -filter-thresh 0.05.
838
839 ***RNA-seq***
840 Total RNA was extracted from finely dissected genital discs or testis samples from 18-25h APF
841 animals using Trizol reagent (Invitrogen). RNA quality was tested by Agilent Bioanalyzer.
842
843 RNA-seq libraries were made using the Illumina Truseq Total RNA library Prep Kit LT.
844 Sequencing was performed on the Illumina Hiseq2500 platform. Following the trimming of
845 adapter sequences with Trimmomatic, RNA-seq reads from replicated wild type (x3) and
846 mutant samples (x3) were aligned to the *Drosophila melanogaster* (dm6) genome assembly
847 utilizing HISAT2. Gene annotations were sourced from UCSC. The DESeq2 Bioconductor
848 package was employed to identify differentially expressed mRNAs between *w1118* and the
849 $ham^{PR\Delta}/ham^{PR\Delta}$ mutant, as well as between +/Df and ham^{SK1}/Df mutant, with a subsequent
850 estimation of the false discovery rate (FDR). Genes with an FDR < 10% and absolute
851 Log2FC>0 were considered differentially expressed. Details of the calculated differential
852 expression are provided in **Supplementary table 5**.
853
854 ***STRING gene network analyses***
855 Ham activated (genes downregulated in *hamSK1* and bound by Ham in TG) and repressed
856 (genes upregulated in *hamSK1* and bound by Ham in TG) gene networks are constructed using
857 String, MCL clustering (find natural clusters the stochastic flow, inflation parameter, 2.
858 Disconnected genes are hidden. The position of the clusters is manually adjusted to fit related
859 GO categories. The links to the gene networks in STRING:
860 https://string-db.org/cgi/network?taskId=bbF8IgMTqf1M&sessionId=bzDIAZvMgWsi
861 https://string-db.org/cgi/network?taskId=bhKCcMoLlbwh&sessionId=bzDIAZvMgWsi
862
863
864
865
866
867

868 **References**

869

870 1. Bernascone, I., M. Hachimi, and F. Martin-Belmonte, *Signaling Networks in Epithelial*
871 *Tube Formation.* Cold Spring Harb Perspect Biol, 2017. **9**(12).
872 2. Chung, S. and D.J. Andrew, *The formation of epithelial tubes.* J Cell Sci, 2008. **121**(Pt
873 21): p. 3501-4.
874 3. Samakovlis, C., et al., *Development of the Drosophila tracheal system occurs by a*
875 *series of morphologically distinct but genetically coupled branching events.*
876 Development, 1996. **122**(5): p. 1395-407.
877 4. Samakovlis, C., et al., *Genetic control of epithelial tube fusion during Drosophila*
878 *tracheal development.* Development, 1996. **122**(11): p. 3531-6.
879 5. Sutherland, D., C. Samakovlis, and M.A. Krasnow, *branchless encodes a Drosophila*
880 *FGF homolog that controls tracheal cell migration and the pattern of branching.* Cell,
881 1996. **87**(6): p. 1091-101.
882 6. Tanaka-Matakatsu, M., et al., *Cadherin-mediated cell adhesion and cell motility in*
883 *Drosophila trachea regulated by the transcription factor Escargot.* Development,
884 1996. **122**(12): p. 3697-705.
885 7. Gervais, L., G. Lebreton, and J. Casanova, *The making of a fusion branch in the*
886 *Drosophila trachea.* Dev Biol, 2012. **362**(2): p. 187-93.
887 8. Jacinto, A., A. Martinez-Arias, and P. Martin, *Mechanisms of epithelial fusion and*
888 *repair.* Nat Cell Biol, 2001. **3**(5): p. E117-23.
889 9. Vasioukhin, V., et al., *Directed actin polymerization is the driving force for epithelial*
890 *cell-cell adhesion.* Cell, 2000. **100**(2): p. 209-19.
891 10. Pai, Y.J., et al., *Epithelial fusion during neural tube morphogenesis.* Birth Defects Res
892 A Clin Mol Teratol, 2012. **94**(10): p. 817-23.
893 11. Caviglia, S. and S. Luschnig, *Tube fusion: making connections in branched tubular*
894 *networks.* Semin Cell Dev Biol, 2014. **31**: p. 82-90.
895 12. de Mello Santos, T. and B.T. Hinton, *We, the developing rete testis, efferent ducts,*
896 *and Wolffian duct, all hereby agree that we need to connect.* Andrology, 2019. **7**(5):
897 p. 581-587.
898 13. Jemc, J.C., *Somatic gonadal cells: the supporting cast for the germline.* Genesis, 2011.
899 **49**(10): p. 753-75.
900 14. DeFalco, T., S. Le Bras, and M. Van Doren, *Abdominal-B is essential for proper*
901 *sexually dimorphic development of the Drosophila gonad.* Mech Dev, 2004. **121**(11):
902 p. 1323-33.
903 15. Whitworth, C., E. Jimenez, and M. Van Doren, *Development of sexual dimorphism in*
904 *the Drosophila testis.* Spermatogenesis, 2012. **2**(3): p. 129-136.
905 16. Ahmad, S.M. and B.S. Baker, *Sex-specific deployment of FGF signaling in Drosophila*
906 *recruits mesodermal cells into the male genital imaginal disc.* Cell, 2002. **109**(5): p.
907 651-61.
908 17. Rothenbusch-Fender, S., et al., *Myotube migration to cover and shape the testis of*
909 *Drosophila depends on Heartless, Cadherin/Catenin, and myosin II.* Biol Open, 2017.
910 **6**(12): p. 1876-1888.
911 18. Fog, C.K., G.G. Galli, and A.H. Lund, *PRDM proteins: important players in*
912 *differentiation and disease.* Bioessays, 2012. **34**(1): p. 50-60.

913 19. Chi, J. and P. Cohen, *The Multifaceted Roles of PRDM16: Adipose Biology and*
914 *Beyond.* Trends Endocrinol Metab, 2016. **27**(1): p. 11-23.
915 20. Bard-Chapeau, E.A., et al., *Ecotopic viral integration site 1 (EVI1) regulates multiple*
916 *cellular processes important for cancer and is a synergistic partner for FOS protein in*
917 *invasive tumors.* Proc Natl Acad Sci U S A, 2012. **109**(6): p. 2168-73.
918 21. Zhou, B., et al., *PRDM16 Suppresses MLL1r Leukemia via Intrinsic Histone*
919 *Methyltransferase Activity.* Mol Cell, 2016.
920 22. Corrigan, D.J., et al., *PRDM16 isoforms differentially regulate normal and leukemic*
921 *hematopoiesis and inflammatory gene signature.* J Clin Invest, 2018. **128**(8): p. 3250-
922 3264.
923 23. Cibi, D.M., et al., *Prdm16 Deficiency Leads to Age-Dependent Cardiac Hypertrophy,*
924 *Adverse Remodeling, Mitochondrial Dysfunction, and Heart Failure.* Cell Rep, 2020.
925 **33**(3): p. 108288.
926 24. Kundu, A., et al., *PRDM16 suppresses HIF-targeted gene expression in kidney cancer.*
927 J Exp Med, 2020. **217**(6).
928 25. Horvath, C. and C. Scheele, *PRDM16 stability and metabolically healthy adipose*
929 *tissue.* Nat Metab, 2022. **4**(9): p. 1095-1096.
930 26. Wang, Q., et al., *Post-translational control of beige fat biogenesis by PRDM16*
931 *stabilization.* Nature, 2022. **609**(7925): p. 151-158.
932 27. Hurwitz, E., et al., *Antagonism between Prdm16 and Smad4 specifies the trajectory*
933 *and progression of pancreatic cancer.* J Cell Biol, 2023. **222**(4).
934 28. Moore, A.W., L.Y. Jan, and Y.N. Jan, *hamlet, a binary genetic switch between single-*
935 *and multiple- dendrite neuron morphology.* Science, 2002. **297**(5585): p. 1355-8.
936 29. Moore, A.W., et al., *Conversion of neurons and glia to external-cell fates in the*
937 *external sensory organs of Drosophila hamlet mutants by a cousin-cousin cell-type*
938 *respecification.* Genes Dev, 2004. **18**(6): p. 623-8.
939 30. Rives-Quinto, N., et al., *Sequential activation of transcriptional repressors promotes*
940 *progenitor commitment by silencing stem cell identity genes.* Elife, 2020. **9**.
941 31. Eroglu, E., et al., *SWI/SNF complex prevents lineage reversion and induces temporal*
942 *patterning in neural stem cells.* Cell, 2014. **156**(6): p. 1259-73.
943 32. Endo, K., et al., *Chromatin modification of Notch targets in olfactory receptor neuron*
944 *diversification.* Nat Neurosci, 2012. **15**(2): p. 224-33.
945 33. Pinheiro, I., et al., *Prdm3 and Prdm16 are H3K9me1 methyltransferases required for*
946 *mammalian heterochromatin integrity.* Cell, 2012. **150**(5): p. 948-60.
947 34. Hohenauer, T. and A.W. Moore, *The Prdm family: expanding roles in stem cells and*
948 *development.* Development, 2012. **139**(13): p. 2267-82.
949 35. Gokcezade, J., G. Sienski, and P. Duchek, *Efficient CRISPR/Cas9 plasmids for rapid and*
950 *versatile genome editing in Drosophila.* G3 (Bethesda), 2014. **4**(11): p. 2279-82.
951 36. Jenett, A., et al., *A GAL4-driver line resource for Drosophila neurobiology.* Cell Rep,
952 2012. **2**(4): p. 991-1001.
953 37. Kaya-Okur, H.S., et al., *CUT&Tag for efficient epigenomic profiling of small samples*
954 *and single cells.* Nat Commun, 2019. **10**(1): p. 1930.
955 38. Szklarczyk, D., et al., *The STRING database in 2023: protein-protein association*
956 *networks and functional enrichment analyses for any sequenced genome of interest.*
957 Nucleic Acids Res, 2023. **51**(D1): p. D638-D646.

958 39. Kozopas, K.M., C.H. Samos, and R. Nusse, *DWnt-2, a Drosophila Wnt gene required*
959 *for the development of the male reproductive tract, specifies a sexually dimorphic cell*
960 *fate.* Genes Dev, 1998. **12**(8): p. 1155-65.
961 40. Deshpande, G., A. Nouri, and P. Schedl, *Wnt Signaling in Sexual Dimorphism.*
962 Genetics, 2016. **202**(2): p. 661-73.
963 41. van Impel, A., et al., *Regulation of the Rac GTPase pathway by the multifunctional*
964 *Rho GEF Pebble is essential for mesoderm migration in the Drosophila gastrula.*
965 Development, 2009. **136**(5): p. 813-22.
966 42. Oda, H., et al., *A Drosophila homolog of cadherin associated with armadillo and*
967 *essential for embryonic cell-cell adhesion.* Dev Biol, 1994. **165**(2): p. 716-26.
968 43. Ferrante, A.W., Jr., R. Reinke, and E.R. Stanley, *Shark, a Src homology 2, ankyrin*
969 *repeat, tyrosine kinase, is expressed on the apical surfaces of ectodermal epithelia.*
970 Proc Natl Acad Sci U S A, 1995. **92**(6): p. 1911-5.
971 44. Gonzalez-Gaitan, M. and H. Jackle, *Role of Drosophila alpha-adaptin in presynaptic*
972 *vesicle recycling.* Cell, 1997. **88**(6): p. 767-76.
973 45. Weber, A.N., et al., *Binding of the Drosophila cytokine Spatzle to Toll is direct and*
974 *establishes signaling.* Nat Immunol, 2003. **4**(8): p. 794-800.
975 46. Staubli, F., et al., *Molecular identification of the insect adipokinetic hormone*
976 *receptors.* Proc Natl Acad Sci U S A, 2002. **99**(6): p. 3446-51.
977 47. Kawamura, K., et al., *A new family of growth factors produced by the fat body and*
978 *active on Drosophila imaginal disc cells.* Development, 1999. **126**(2): p. 211-9.
979 48. Lam, G.T., C. Jiang, and C.S. Thummel, *Coordination of larval and prepupal gene*
980 *expression by the DHR3 orphan receptor during Drosophila metamorphosis.*
981 Development, 1997. **124**(9): p. 1757-69.
982 49. Prokopenko, S.N., et al., *A putative exchange factor for Rho1 GTPase is required for*
983 *initiation of cytokinesis in Drosophila.* Genes Dev, 1999. **13**(17): p. 2301-14.
984 50. Nakamura, M., J.M. Verboon, and S.M. Parkhurst, *Prepatterning by RhoGEFs governs*
985 *Rho GTPase spatiotemporal dynamics during wound repair.* J Cell Biol, 2017. **216**(12):
986 p. 3959-3969.
987 51. Lin, Y.H., et al., *AP-2-complex-mediated endocytosis of Drosophila Crumbs regulates*
988 *polarity by antagonizing Stardust.* J Cell Sci, 2015. **128**(24): p. 4538-49.
989 52. Campbell, K. and J. Casanova, *A role for E-cadherin in ensuring cohesive migration of*
990 *a heterogeneous population of non-epithelial cells.* Nat Commun, 2015. **6**: p. 7998.
991 53. Chen, H., et al., *E-cadherin mediates adhesion and suppresses cell motility via distinct*
992 *mechanisms.* J Cell Sci, 1997. **110 (Pt 3)**: p. 345-56.
993 54. Sountoulidis, A., et al., *SCRINSHOT enables spatial mapping of cell states in tissue*
994 *sections with single-cell resolution.* PLoS Biol, 2020. **18**(11): p. e3000675.
995 55. Umetsu, D., *Cell mechanics and cell-cell recognition controls by Toll-like receptors in*
996 *tissue morphogenesis and homeostasis.* Fly (Austin), 2022. **16**(1): p. 233-247.
997 56. Karlsson, M., et al., *A single-cell type transcriptomics map of human tissues.* Sci Adv,
998 2021. **7**(31).
999 57. Corty, M.M., B.J. Matthews, and W.B. Grueber, *Molecules and mechanisms of*
1000 *dendrite development in Drosophila.* Development, 2009. **136**(7): p. 1049-61.
1001 58. Araujo, S.J. and J. Casanova, *Sequoia establishes tip-cell number in Drosophila*
1002 *trachea by regulating FGF levels.* J Cell Sci, 2011. **124**(Pt 14): p. 2335-40.

59. Brenman, J.E., et al., *Sequoia, a tramtrack-related zinc finger protein, functions as a pan-neural regulator for dendrite and axon morphogenesis in Drosophila.* Dev Cell, 2001. **1**(5): p. 667-77.
60. Araujo, S.J., C. Cela, and M. Llimargas, *Tramtrack regulates different morphogenetic events during Drosophila tracheal development.* Development, 2007. **134**(20): p. 3665-76.
61. Li, S., et al., *Photoreceptor cell differentiation requires regulated proteolysis of the transcriptional repressor Tramtrack.* Cell, 1997. **90**(3): p. 469-78.
62. Pitsouli, C. and N. Perrimon, *The homeobox transcription factor cut coordinates patterning and growth during Drosophila airway remodeling.* Sci Signal, 2013. **6**(263): p. ra12.
63. Grueber, W.B., L.Y. Jan, and Y.N. Jan, *Different levels of the homeodomain protein cut regulate distinct dendrite branching patterns of Drosophila multidendritic neurons.* Cell, 2003. **112**(6): p. 805-18.
64. Meers, M.P., D. Tenenbaum, and S. Henikoff, *Peak calling by Sparse Enrichment Analysis for CUT&RUN chromatin profiling.* Epigenetics Chromatin, 2019. **12**(1): p. 42.

Declaration of the use of AI. ChatGPT was used to improve readability of the text, and the content was thoroughly checked and edited by the authors to ensure accuracy.

1041 **Figure legends**

1042

1043 **Figure 1. *ham* is expressed and required for *Drosophila* male RS development**

1044

1045 (**A**). Illustration of the developing male RS. The testis (TE) terminal epithelial cells localize at
1046 the opposite side of the germline stem cell niche. The genital disc (GD) contains mesenchymal
1047 cells (MC) that will develop into the SV and accessory gland (ag). (**B**). Illustration of the TE
1048 and SV fusion process. APF, after pupal formation. (**C**). The adult male RS. ejd, ejaculatory
1049 duct. (**D**). White-field images of adult male RS, showing defective morphology in the *ham*
1050 mutants. (**E**). Quantification of male fertility. Ham_sfGFP with the *ham* genomic region was
1051 used to rescue the sterility. Statistical significance was calculated using unpaired t-test (***,
1052 $p<0.001$; **, $p< 0.01$; *, $p<0.05$; n.s., non-significant). (**F**). Images of the adult RS stained with
1053 Ham_V5 in red. DNA is stained with DAPI in blue. (**G**). Images of the larval TE (top) and
1054 GD (bottom) stained with Ham_V5 in red, the reporter in green (btlGal4 driving UAS-GFP)
1055 and DAPI in blue. AEL, after egg laying. (**H**). Images of the pupal GD stained with Ham_V5
1056 in red, the reporter in green (btlGal4 driving UAS-GFP) and DAPI in blue. APF, after pupal
1057 formation. (**I**) Images of the pupal RS with Ham_V5 in red and DAPI in blue. (**J**). Higher
1058 magnification image of the joint site between the SV and TE, with myoblasts labeled by
1059 mef2Gal4>GFP.

1060

1061 **Figure 2. Ham promotes differentiation of the TE terminal and SV epithelial cells**

1062 (**A**). Images of the male RS at the pupal stage, showing morphological defects of the TE and
1063 SV in the ham mutants. Epithelial cells are labeled with Coracle (Cor). (**B**). High magnification
1064 images of the connection site of the TE and SV, showing that the ham mutant RS failed to form
1065 a continuous tube. Ham-sfGFP restored the normal morphology. Epithelial cells are marked by
1066 E-Cad in red, Cor in yellow, and the epithelium on the SV side also marked by btlGal4 driving
1067 UAS-mCD8GFP. DNA is labeled by DAPI in blue. (**C**). Images and quantification of the E-
1068 Cad signal in the *wt* and *hamPRΔ* mutant SV. (**D**). Images and quantification of the Crumbs
1069 signal in the *wt* and *hamPRΔ /Df* mutant SV. (**E**). Images and quantification of the length of
1070 Cor signal in the wt and *hamPRΔ* mutant SV. (**F**) Images of *ham* mutant mosaic clones in the
1071 TE terminal epithelial cells. Note, the mutant cells are GFP negative and within the area
1072 surrounded by the white dashed line. The white arrows indicate junctions between mutant cells,
1073 while the yellow arrows highlight the junctions between wild-type cells. (**G**). Images of pupal
1074 male GD, showing that *hamRNAi*-mediated knockdown reproduces *ham* mutant phenotypes.

1075 (**H**). Images of pupal male RS, stained with E-Cad in red, Ham in yellow, GFP in green and
1076 DAPI in blue. UAS-dcr2 enhanced knockdown efficiency and led to more severe
1077 morphological defects. (**I**). Images and quantification of E-Cad signal in red and Cor length in
1078 blue in control and ham RNAi SV. (**J**) Images and quantification of E-Cad signal in control
1079 and ham RNAi TE terminal epithelium. Statistical significance was calculated using unpaired
1080 t-test except for TE mosaic clones which used paired t-test. (***, p<0.001; **, p< 0.01; *,
1081 p<0.05; ns, non-significant).
1082
1083 **Figure 3. Identification of Ham-regulated genes in the developing TE and GD**
1084
1085 (**A**). Illustration of the sample types and antibodies used in the RNA-seq and CUT&TAG
1086 experiments. (**B**) Venn diagram of dysregulated genes between the two mutant conditions in
1087 the GD (left) and TE (right) samples. (**C**) Heatmaps of Ham CUT&TAG peak density and IgG
1088 control, ranked from high to low and centered at peak summits. (**D**) Venn diagrams of
1089 CUT&TAG peaks from the two types of samples. (**E-F**). Volcano plots of dysregulated genes
1090 in GD (E) and TE (F) in the *hamSK1/Df* mutant, and the ones with at least one Ham CUT&TAG
1091 peak are highlighted.
1092
1093 **Figure 4. Ham activates expression of epithelial differentiation genes**
1094
1095 (**A**) Ham gene network analysis from STRING. The position of MCL Clusters were manually
1096 adjusted to place genes with similar function in close proximity. The functional categories were
1097 determined by gene function tools in STRING. (**B**). A bar plot of the Log2 fold-change value
1098 from RNA-seq for *wnt2*, *shot* and *shg*, showing downregulation of these genes in the
1099 *hamSK1/Df* mutant. (**C**). Schemes of the Ham_FL and other truncation proteins, and illustration
1100 of the luciferase reporter assay. (**D, F**). A genome browser snapshot of the *shg* and *wnt2* loci,
1101 showing the CUT&TAG tracks from the TE and GD (TG) mixed samples and the enhancer
1102 fragments in the luciferase assays. (**E, G**). Normalized luciferase activity to the empty reporter
1103 and then to the control vector that expresses GFP and RFP proteins. Statistical significance was
1104 calculated using unpaired t-test (****, p<0.0001; ***, p<0.001; **, p< 0.01; *, p<0.05; ns,
1105 non-significant).
1106
1107 **Figure 5. A candidate RNAi screen identified Ham-downstream effectors in RS epithelial**
1108 **tissue fusion**

1109

1110 (**A**). Scheme for the RNAi screen. (**B**) Summary of positive hits. The extent of sterility is
1111 determined by the number of progenies from the F1 male crossing to the wild-type female (see
1112 Methods). 100% means no progeny. >70%, the number of progenies being fewer than 30% of
1113 the number of progenies produced by the control cross (the same Gal4 driver x UAS-
1114 GFPRNAi). 40-70%, the number of progenies being between 30-60% of the number of
1115 progenies produced by the control. (**C**). Images of the control and gene-specific RNAi
1116 knockdown RS. The left panels show the fusion site stained with E-Cad in red, GFP in green,
1117 Ham in yellow and DAPI in blue, the middle panels are GD, and the right ones are TE. The
1118 orange arrows indicate mobilized epithelial cells in the *shg* knockdown TE.

1119

1120 **Figure 6. Spatial-temporal expression dynamics of Ham-downstream genes**

1121

1122 (**A**). Images from multiplexed in situ hybridization (the SCRINSHOT method), showing
1123 mRNA signal of the indicated genes in *wt* TE samples. DNA is marked by DAPI in grey. (**B**).
1124 Images from SCRINSHOT, showing mRNA signals of indicated genes in *wt/Df* and
1125 *hamSK1/Df* mutant GD. The last panel is an enlarged view from the sample with *Tl*, *ham* and
1126 *spz* probes. The yellow arrowheads indicate myoblast cells with Tl signal. (**C**). Quantification
1127 of signal intensity for genes shown in B in two areas, the SV and EjD. Statistical significance
1128 was calculated using unpaired t-test (***, $p<0.001$; **, $p< 0.01$; *, $p<0.05$; ns, non-significant).
1129 (**D**) Images from SCRINSHOT, showing mRNA signals of indicated genes in *GFP* and *ham*
1130 *RNAi* GD samples. (**E**). Quantification of signal intensity for genes shown in D in two areas,
1131 the SV and EjD. (**F**). A summary of genes expressed in the TE terminal and SV epithelium.
1132 Highlighted genes show temporal or spatial dynamic expression in the two tissues. Statistical
1133 significance was calculated using unpaired t-test (****, $p<0.0001$; ***, $p<0.001$; **, $p< 0.01$;
1134 *, $p<0.05$; ns, non-significant).

1135

1136 **Figure 7. Wnt2 and its ligand genes are required for male fertility and RS development**
1137 (**A**) Images of *wnt2o* mutant TE and GD, showing disrupted morphology in these tissues. (**B**).
1138 Images of the TE and SV fusion site from the control and *wnt2* overexpression animals. The
1139 epithelial cells of the TE and SV are labeled with hamRSGal4 driving UAS-mCD8GFP in
1140 green and E-Cad in red and Ham in yellow. The white arrows indicate mobilized GFP positive
1141 cells in the middle of the TE, and these cells have a lower level of E-Cad. (**C**). Images of the
1142 TE and SV fusion site from the control and *fz2* RNAi animals. The white arrows indicate

1143 mobilized GFP positive cells in the middle of the TE, and these cells have a lower level of E-
1144 Cad. (**D**) Graphs of progeny number from male fertility tests for *fz* and *fz2* RNAi lines in
1145 comparison to GFP RNAi. Number of tested males in each genotype, 3. (**E**) Illustration of cell-
1146 cell interactions in the developing RS, and a speculated model for Tl and Wnt2 signaling
1147 functions. Wnt2 signaling may be involved in epithelial cell interaction between the two ends.
1148 Tl signaling and Tl may be involved in the interaction between epithelial cells and myoblasts.
1149 In three conditions (*shgRNAi*, *wnt2OE* and *fz2RNAi*), some TE terminal epithelial cells
1150 (illustrated in orange) move up to the distal end of the testis.
1151
1152
1153
1154

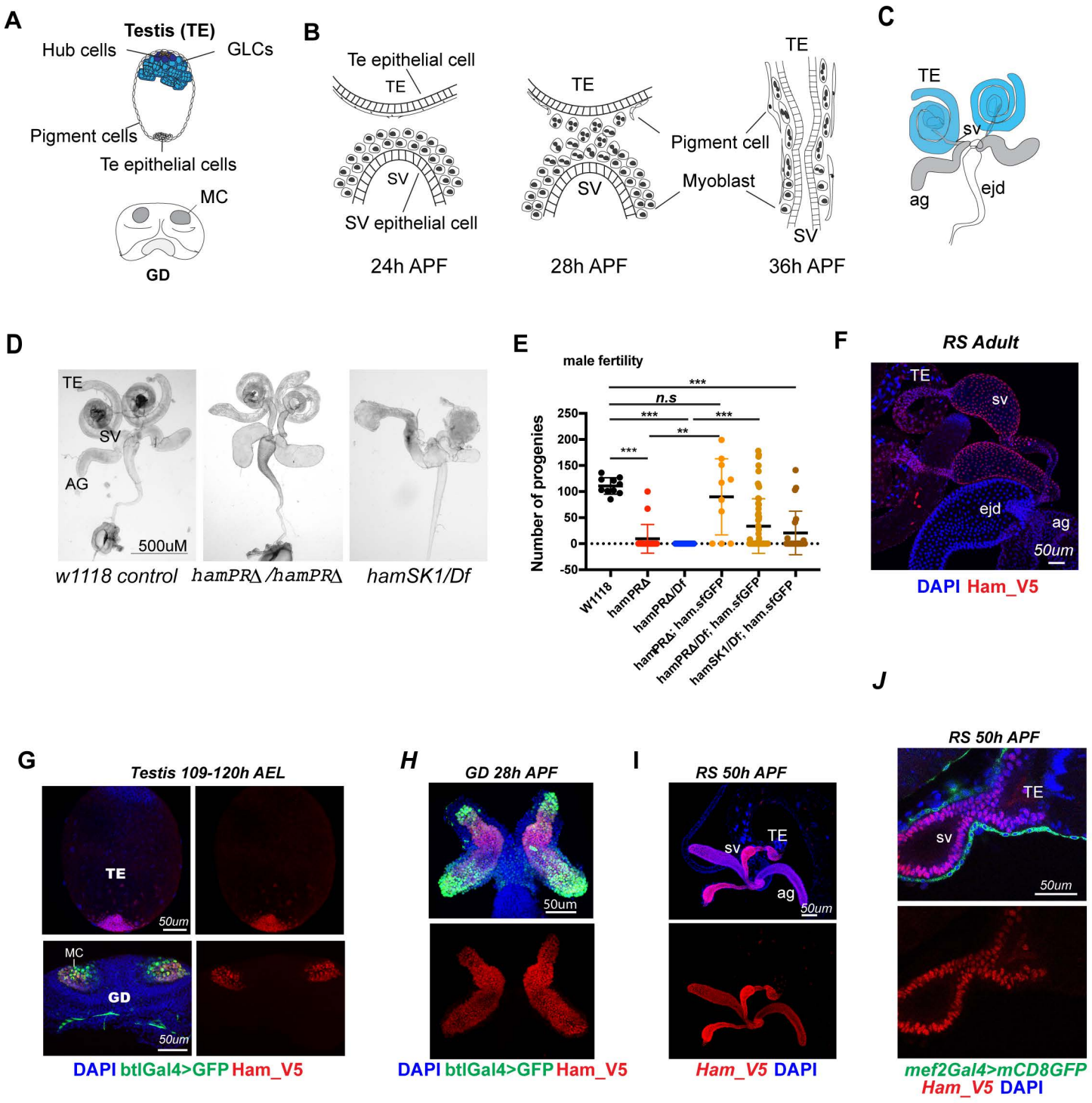
A
Testis (TE)
Hub cells
GLCs
Pigment cells
Te epithelial cells
MC
GD
B
Te epithelial cell
TE
SV
SV epithelial cell
24h APF
TE
SV
Pigment cell
Myoblast
28h APF
TE
SV
36h APF
C
TE
sv
ag
ejd
D
TE
SV
AG
500uM
w1118 control
hamPRΔ/hamPRΔ
hamSK1/Df
E
male fertility
Number of progenies
n.s
***
**
W1118
hamPRΔ
hamPRΔ/Df
hamPRΔ; ham.sfGFP
hamPRΔ/Df; ham.sfGFP
hamSK1/Df; ham.sfGFP
F
RS Adult
TE
sv
ejd
ag
50um
DAPI Ham_V5
G
Testis 109-120h AEL
TE
MC
GD
50um
DAPI btlGal4>GFP Ham_V5
H
GD 28h APF
50um
DAPI btlGal4>GFP Ham_V5
I
RS 50h APF
TE
sv
ag
50um
Ham_V5 DAPI
J
RS 50h APF
TE
sv
50um
mef2Gal4>mCD8GFP
Ham_V5 DAPI

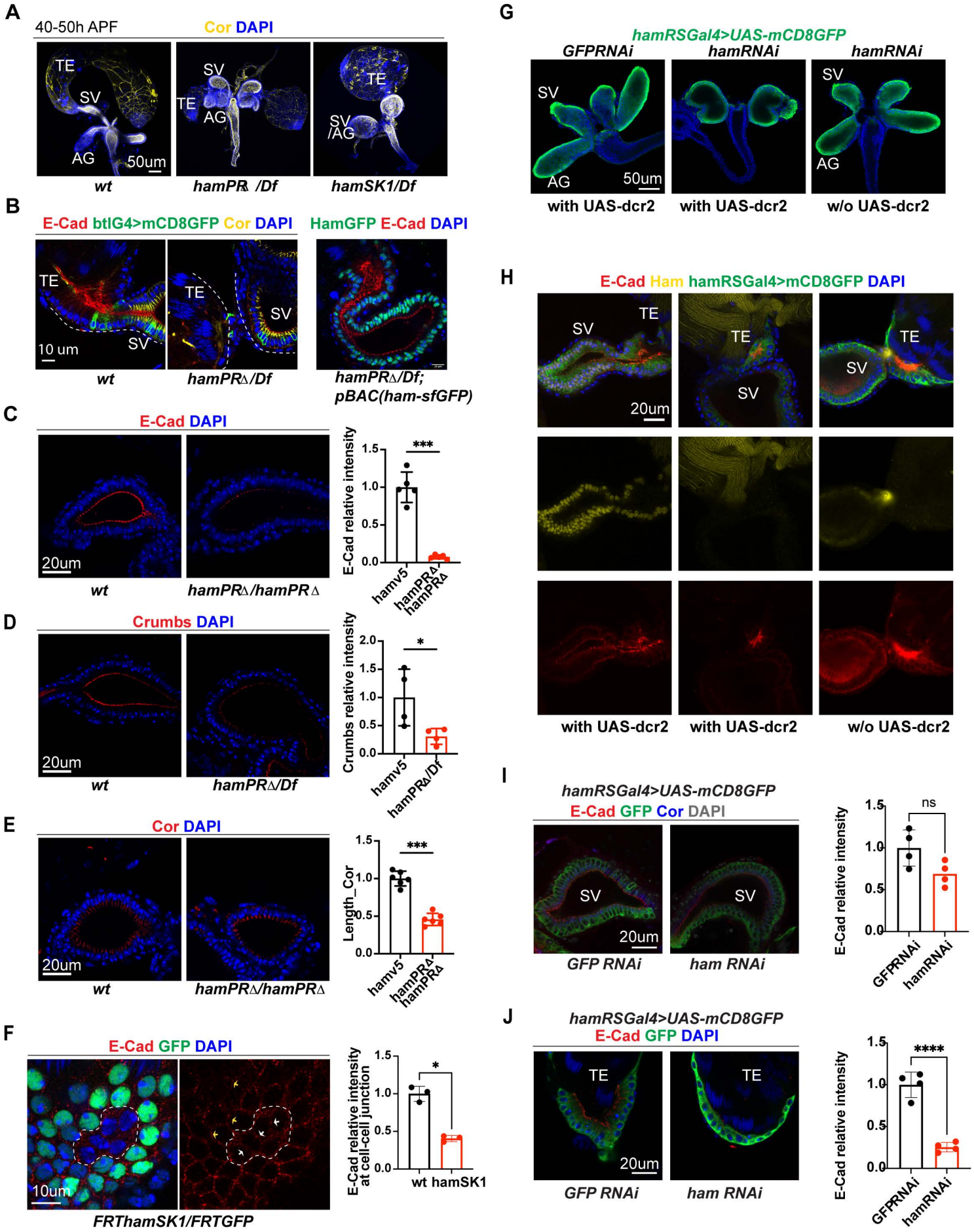
A
40-50h APF
Cor DAPI
TE
SV
AG
50um
wt
hamPRΔ /Df
hamSK1/Df
B
E-Cad btlG4>mCD8GFP Cor DAPI
HamGFP E-Cad DAPI
10 um
hamPRΔ/Df
hamPRΔ/Df;
pBAC(ham-sfGFP)
C
E-Cad DAPI
20um
hamPRΔ/hamPRΔ
E-Cad relative intensity
hamv5
D
Crumbs DAPI
Crumbs relative intensity
hamPRΔ/Df
E
Cor DAPI
Length_Cor
F
E-Cad GFP DAPI
10um
FRThamSK1/FRTGFP
E-Cad relative intensity at cell-cell junction
wt hamSK1
G
hamRSGal4>UAS-mCD8GFP
GFPRNAi
hamRNAi
with UAS-dcr2
w/o UAS-dcr2
H
E-Cad Ham hamRSGal4>mCD8GFP DAPI
I
hamRSGal4>UAS-mCD8GFP
E-Cad GFP Cor DAPI
GFP RNAi
ham RNAi
ns
J
E-Cad GFP DAPI

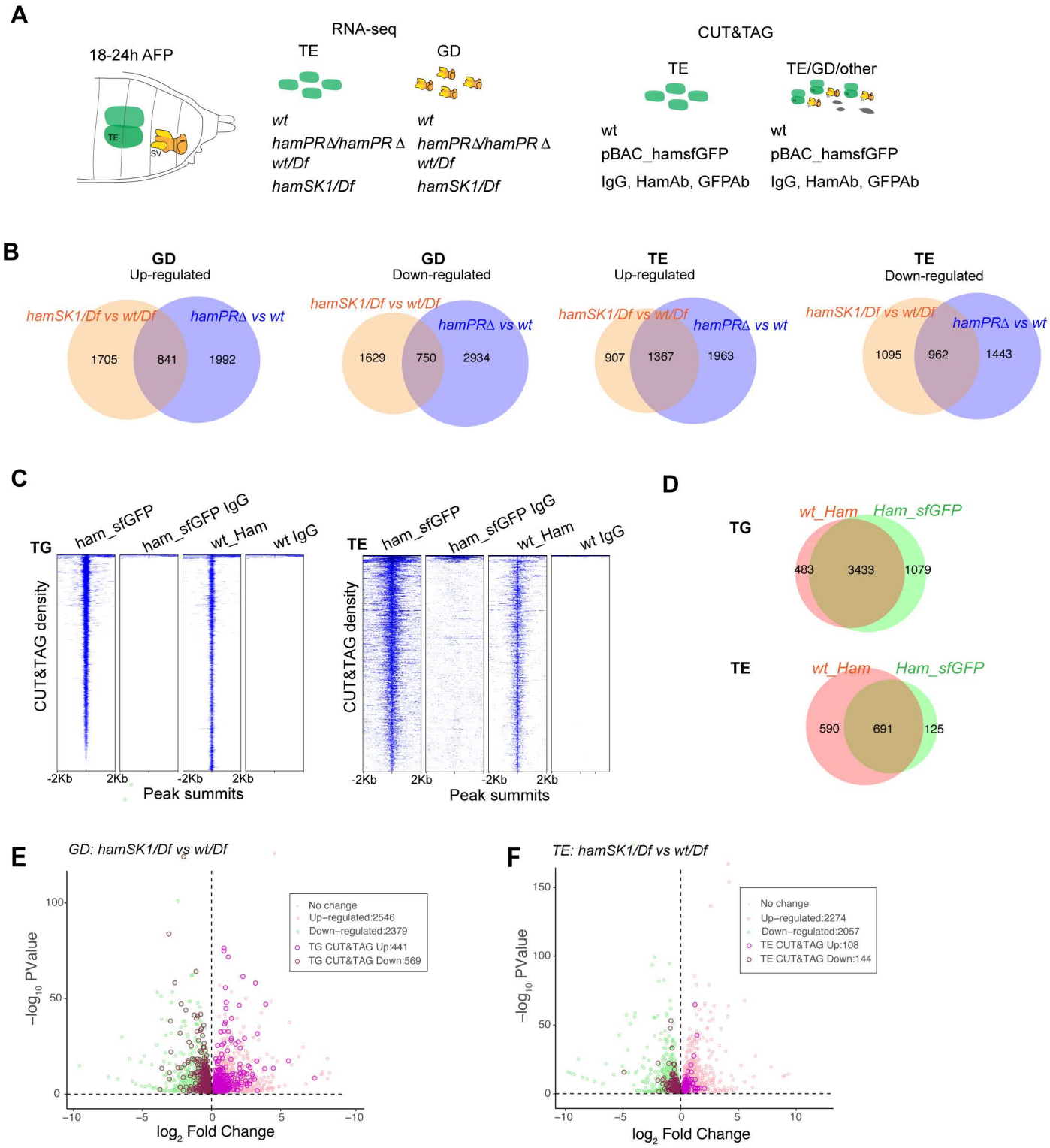
A
18-24h AFP
TE
SV
RNA-seq
TE
GD
wt
hamPRΔ/hamPR Δ
wt/Df
hamSK1/Df
wt
hamPRΔ/hamPR Δ
wt/Df
hamSK1/Df
CUT&TAG
TE
TE/GD/other
wt
pBAC_hamsfGFP
IgG, HamAb, GFPAb
wt
pBAC_hamsfGFP
IgG, HamAb, GFPAb
B
GD
Up-regulated
hamSK1/Df vs wt/Df
hamPRΔ vs wt
1705
841
1992
GD
Down-regulated
hamSK1/Df vs wt/Df
hamPRΔ vs wt
1629
750
2934
TE
Up-regulated
hamSK1/Df vs wt/Df
hamPRΔ vs wt
907
1367
1963
TE
Down-regulated
hamSK1/Df vs wt/Df
hamPRΔ vs wt
1095
962
1443
C
TG
ham_sfGFP
ham_sfGFP IgG
wt_Ham
wt IgG
CUT&TAG density
-2Kb
2Kb
Peak summits
TE
ham_sfGFP
ham_sfGFP IgG
wt_Ham
wt IgG
CUT&TAG density
-2Kb
2Kb
Peak summits
D
TG
wt_Ham
Ham_sfGFP
483
3433
1079
TE
wt_Ham
Ham_sfGFP
590
691
125
E
GD: hamSK1/Df vs wt/Df
No change
Up−regulated:2546
Down−regulated:2379
TG CUT&TAG Up:441
TG CUT&TAG Down:569
−log10 PValue
log2 Fold Change
F
TE: hamSK1/Df vs wt/Df
No change
Up−regulated:2274
Down−regulated:2057
TE CUT&TAG Up:108
TE CUT&TAG Down:144
−log10 PValue
log2 Fold Change

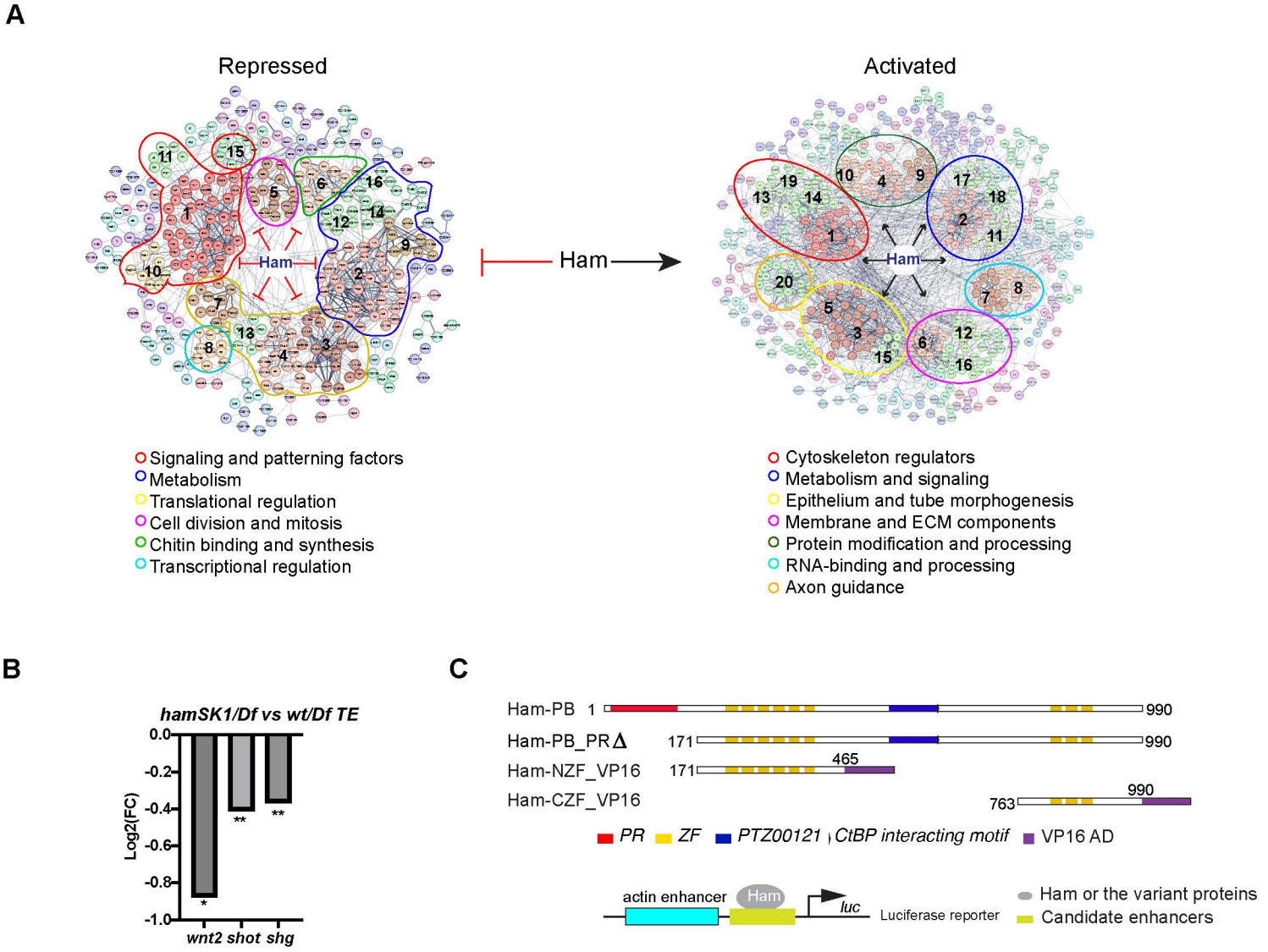
A
Repressed
Activated
Ham
Ham
Signaling and patterning factors
Metabolism
Translational regulation
Cell division and mitosis
Chitin binding and synthesis
Transcriptional regulation
Cytoskeleton regulators
Metabolism and signaling
Epithelium and tube morphogenesis
Membrane and ECM components
Protein modification and processing
RNA-binding and processing
Axon guidance
B
hamSK1/Df vs wt/Df TE
Log2(FC)
wnt2 shot shg
C
Ham-PB
Ham-PB_PRΔ
Ham-NZF_VP16
Ham-CZF_VP16
PR
ZF
PTZ00121
CtBP interacting motif
VP16 AD
actin enhancer
Ham
luc
Luciferase reporter
Ham or the variant proteins
Candidate enhancers
D
shg_enh2-1
shg
CG15653
cpa
HamGFP_TG1_GFP
HamGFP_TG2_GFP
wt_TG2_Ham
E
wnt2_enh1-4
wnt2
HamGFP_TG1_GFP
HamGFP_TG2_GFP
wt_TG2_Ham
F
Normalized luciferase activity
GFP-RFP
Ham_FL
Ham_PRdel
Ham_NZF_VP16
Ham_CZF_VP16
shg_enh1
enh2
G
Normalized luciferase activity
GFP-RFP
Ham_FL
Ham_PRdel
Ham_NZF_VP16
Ham_CZF_VP16
wnt2_enh1
enh2
enh3
enh4

A

hamRSGal4>UAS-dcr2; UAS-mCD8GFP

X

UAS-RNAi
(135 lines for 113 genes)

↓

Screen for F1 male sterility

↓

26 positive gene hits

B

Sterility	Genes
100%	*pbl, AP-2alpha, CG11406, shg*
>70%	*GstE11, CG7456, Gr64c, AkhR, Idgf4*
40%-70%	*CG17477, CG11069, CG17186, CG4872, AdSL, Tl, CG17283, decay, PH4alphaMP, Hr46, CG15117, gsb-n, shark, CG17018, cag, CG7484, CG31935*

C

hamRSGal4;UASmCD8GFP **E-Cad GFP Ham DAPI**

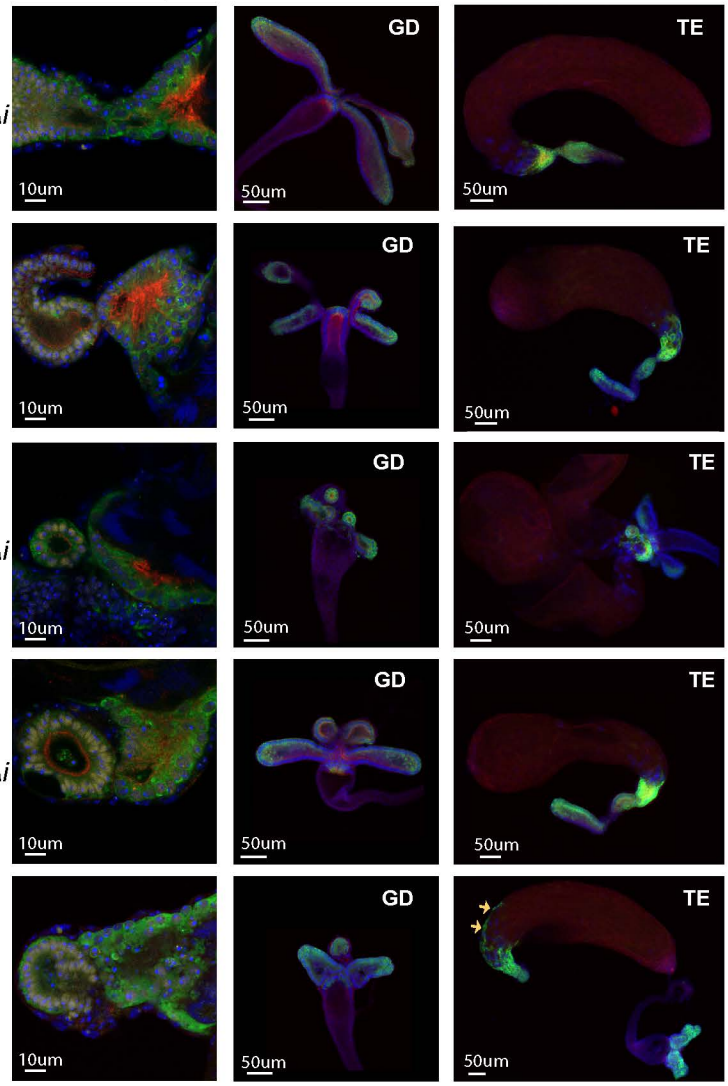

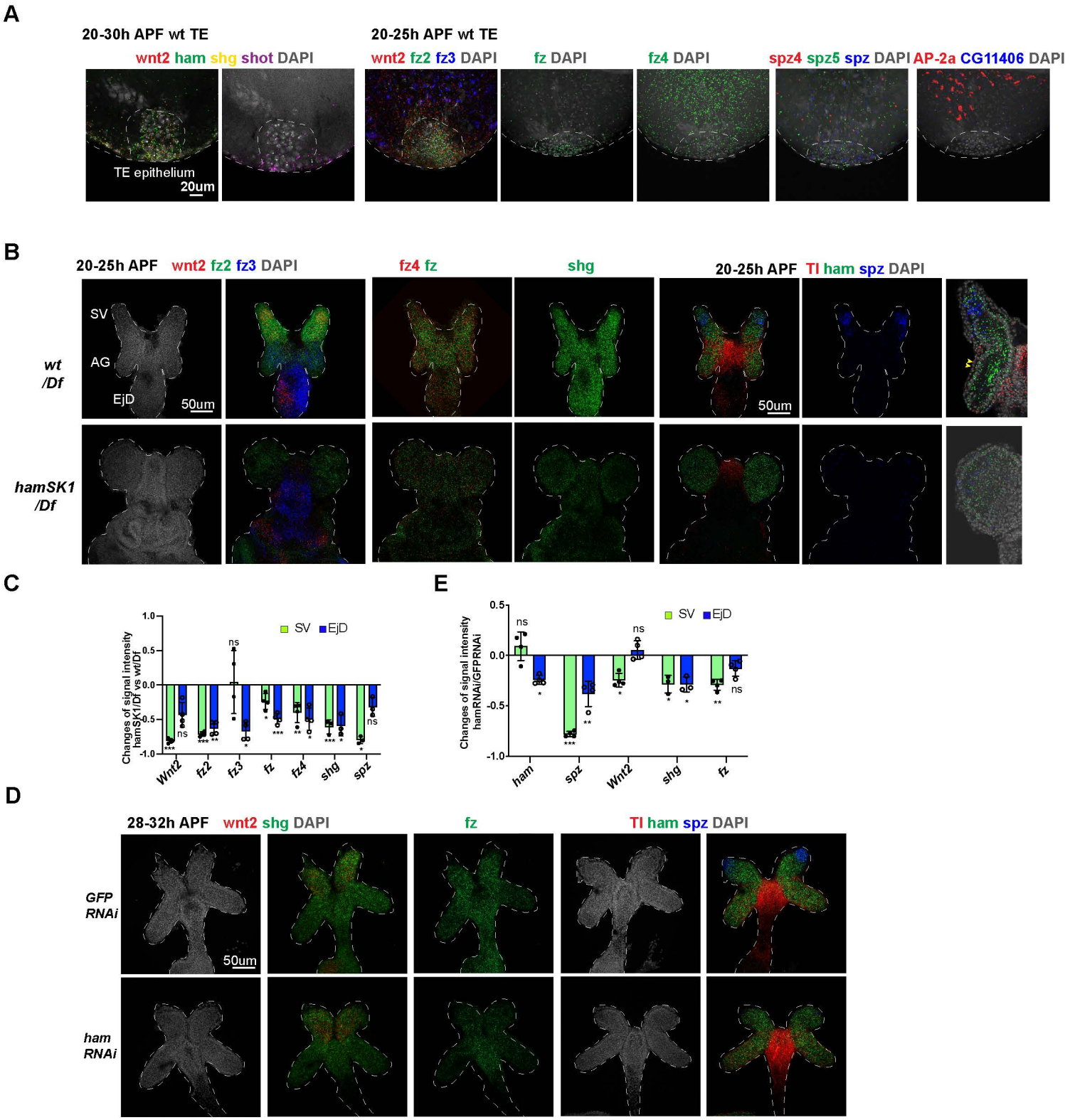
A
20-30h APF wt TE
wnt2 ham shg shot DAPI
TE epithelium
20um
20-25h APF wt TE
wnt2 fz2 fz3 DAPI
fz DAPI
fz4 DAPI
spz4 spz5 spz DAPI
AP-2a CG11406 DAPI
B
20-25h APF wnt2 fz2 fz3 DAPI
fz4 fz
shg
20-25h APF Tl ham spz DAPI
SV
AG
EjD
50um
wt /Df
hamSK1 /Df
C
SV EjD
Changes of signal intensity hamSK1/Df vs wt/Df
Wnt2 fz2 fz3 fz fz4 shg spz
E
SV EjD
Changes of signal intensity hamRNAi/GFPRNAi
ham spz Wnt2 shg fz
D
28-32h APF wnt2 shg DAPI
fz
Tl ham spz DAPI
GFP RNAi
ham RNAi
50um
F
TE
SV
Tl
TE epithelium
Constant genes:
ham, shg, shot, wnt2, fz, fz2, fz4, spz, AdSL, Shark, CG7456
Early genes:
spz5, CG11406
Late genes:
Tl, spz6, Ap2-a, GstE11
SV epithelium
Shared with TE:
ham, shg, shot, wnt2, fz, fz2, fz4, spz, spz6, AdSL, Shark, spz5, CG7456, GstE11, AP2-a, CG11406
Unique in SV:
CG11069, CG31935,CG17186, fz3, spz4, Gr64c, Cag, CG7484

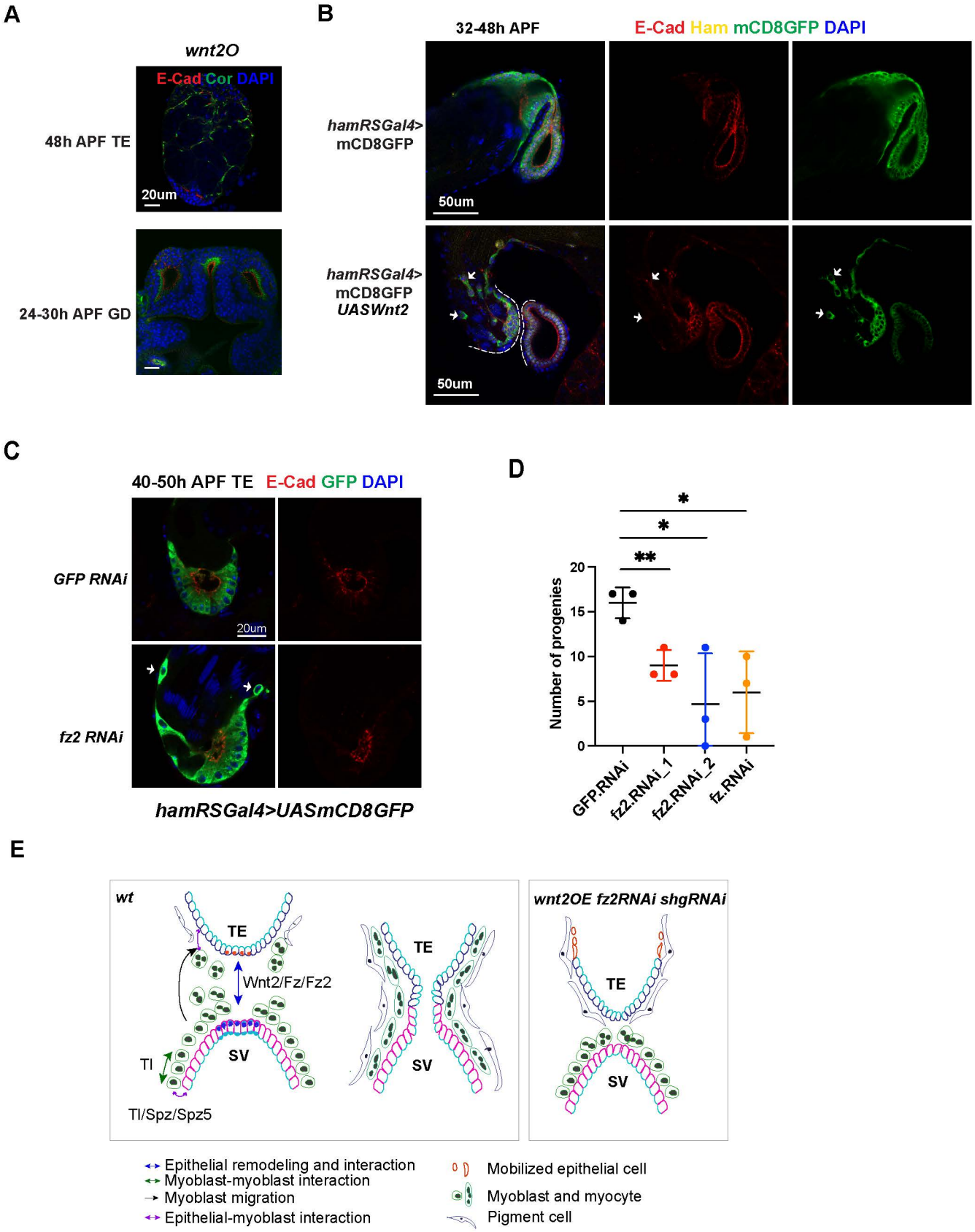
A
wnt2O
E-Cad Cor DAPI
48h APF TE
20um
24-30h APF GD
B
32-48h APF
E-Cad Ham mCD8GFP DAPI
hamRSGal4>
mCD8GFP
50um
hamRSGal4>
mCD8GFP
UASWnt2
50um
C
40-50h APF TE E-Cad GFP DAPI
GFP RNAi
20um
fz2 RNAi
hamRSGal4>UASmCD8GFP
D
Number of progenies
20
15
10
5
0
*
*
**
GFP.RNAi
fz2.RNAi_1
fz2.RNAi_2
fz.RNAi
E
wt
TE
Wnt2/Fz/Fz2
SV
Tl
Tl/Spz/Spz5
TE
SV
wnt2OE fz2RNAi shgRNAi
TE
SV
Epithelial remodeling and interaction
Myoblast-myoblast interaction
Myoblast migration
Epithelial-myoblast interaction
Mobilized epithelial cell
Myoblast and myocyte
Pigment cell